Asia-Pacific Journal of Atmospheric Sciences (2025) 61:19
https://doi.org/10.1007/s13143-025-00404-9

Online ISSN 1976-7951
Print ISSN 1976-7633

ORIGINAL ARTICLE

A Case Study Simulation of the Heavy Rainfall Event in Southwestern Taiwan during the Mei-Yu Front on May 22, 2020

Jou-Ping Hou[1] · **Chih-Yi Chen**[1] · **Pei-Di Jeng**[1]

Received: 5 December 2024 / Revised: 23 April 2025 / Accepted: 26 May 2025 / Published online: 26 June 2025

Abstract

On May 22, 2020, Qiaotou Meteorological Station in Kaohsiung City of southern Taiwan recorded 415.5 mm of daily rainfall. This heavy rainfall event was driven by the Mei-yu front, a strong and moist southwesterly flow, a mesoscale convective system (MCS), and the complex terrain of southern Taiwan. The study indicates that on May 22, the low-level jet (LLJ) intensified to southwesterly flow strength, rapidly bringing abundant moisture to southwestern Taiwan, resulting in higher equivalent potential temperatures in the lower atmosphere. This study, through observational data analysis and case simulation, found that the first important cause of heavy rainfall in southwestern Taiwan is the presence of a strong southwesterly LLJ in an unstable atmospheric environment, which transports abundant moisture to the land in southwestern Taiwan. At the same time, the lifting mechanisms ahead of the Mei-yu front and low-level convergence over the ocean contribute to the intensification of the MCS. The second factor is Taiwan's complex terrain effects, which functioned as a barrier to moisture transport and enhanced orographic lifting on the windward side, further intensifying the rainfall when combined with the strong southwesterly flow and MCS. Numerical simulations show that under the influence of complex terrain, mean precipitation over the southern section of Taiwan's Central Mountain Range increases from north to south as elevation decreases, the average precipitation gradually decreases when the terrain is below 1100 m. For mountains between 2000 and 2500 m, maximum precipitation occurs on the windward slopes or in front of mountains, while rainfall and moisture sharply decrease on the leeward side. For elevations between 1000 and 1500 m, mean precipitation on the windward slopes increases, with the peak shifting closer to the mountain tops. Below 1000 m, mean precipitation decreases but aligns with the terrain, with the maximum near the peaks. At elevations below 600 m, leeward mean precipitation was above average.

Keywords Mei-yu front · Southwesterly flow · MCS · Heavy rainfall · Low-level jet · Terrain effects

1 Introduction

The Mei-yu, a seasonal weather phenomenon of East Asia, is typically defined from mid-May to mid-June in Taiwan. The Mei-yu front, a quasi-stationary subtropical front often accompanied by organized mesoscale convective systems (MCS), frequently produces repetitive rainfall events during its stationary periods (Chen 2004; Chen and Chen 2003). A relatively weak horizontal air temperature gradient characterizes the Mei-yu front, yet accompanied by abundant moisture, enhancing the gradient of equivalent potential temperature (Ding 1992). During the Mei-yu season, the large-scale atmospheric circulation over Taiwan is characterized by a southwesterly flow intensifying with height. In the post-frontal region, cooler northeasterly winds dominate, with a depth of approximately 1 km (Chen and Hui 1990, 1992). The combination of low- to mid-level atmospheric wind shear, conditionally unstable air, and abundant moisture provides favorable conditions for the formation of organized MCS near the Mei-yu front (Wang et al. 1990; Lin et al. 1990). Previous studies have indicated that during the Mei-yu season, the marine boundary layer jet (MBLJ) below 900 hPa plays a crucial role in precipitation over Taiwan (Tu et al. 2019, 2020). The presence of conditional

✉ Jou-Ping Hou
hoedwardho@gmail.com

[1] Department of Environmental and Information Engineering, Chung Cheng Institute of Technology, National Defense University, No.75, Shiyuan Rd., Daxi Township, Taoyuan County 33551, Taiwan (R.O.C.)

symmetric instability enhances the transport efficiency of the low-level jet (LLJ), allowing the transfer of abundant moisture to the frontal region and supporting the sustained development of convection and precipitation (Chen et al. 1996). MCS formation is typically closely associated with frontal systems, moisture transport by LLJs, and terrain effects. When the Mei-yu front converges with the LLJ on its southern side, substantial moisture accumulates around Taiwan, creating favorable latent heat release conditions for MCS development. Additionally, the alternation of land-sea breezes is crucial in maintaining and enhancing MCS development. In the structure of MCS, updrafts frequently develop in the leading region, lifting warm, moist air to higher levels, where water vapor condensation generates obvious precipitation. The rear-to-front flow of MCS, enhances moisture transport within the convective system, supporting increased precipitation intensity. The interaction between the updrafts and the rear-to-front flow results in the formation of a concentrated rain band in the leading region of the MCS, further enhancing precipitation (Chen 1992).

The southwesterly airflow or LLJ transports moist and creates thermodynamically unstable air condition to Taiwan. Under low-level convergence and vertical wind shear vorticity conditions, this unstable air is lifted, initiating MCSs. As these systems move inland, the orographic features of southwestern Taiwan further intensify the convective systems and contribute to heavy rainfall events (Chien 2015). Chien and Chiu (2023) found that stronger southwesterly airflow leads to heavier rainfall in southern Taiwan. During the 36 h from 0000 UTC on May 21 to 1200 UTC on May 22, 2020, strong westerly winds flowed along the southern edge of the Tibetan Plateau and moved into the low-level land plains of southwestern China, forming a southwest vortex (SWV). As the vortex moved eastward, the strong southwesterly winds on its southern side combined with the monsoonal southwesterly airflow, continuously transporting moisture to Taiwan. The interaction between the intense southwesterly airflow and the eastward movement of a SWV further enhanced moisture transport to Taiwan. This, combined with the lifting effect of the Mei-yu front, triggered heavy rainfall events in southern Taiwan. Additionally, the study suggested that topography is another key factor influencing regional rainfall, although it was not discussed in detail.

During the Mei-yu season, extreme rainfall in Taiwan is influenced by topography and prevailing wind directions. In particular, when westerly and southwesterly winds dominate, both overall rainfall and extreme precipitation trends obviously increase across western side of Taiwan. This effect is especially obvious on the windward slopes of the southwestern Central Mountain Range, where precipitation far exceeds that in other regions (Henny et al. 2021). The topography of the Central Mountain Range has a substantial impact on the spatial distribution of precipitation, particularly enhancing rainfall on the windward slopes (Chen and Chen 2003; Chen et al. 2007). On June 14, 2008, a pre-frontal squall line system and its accompanying rainband passed over Taiwan, resulting in daily rainfall exceeding 100 mm in southwestern Taiwan. During 1100–1300 UTC that day, precipitation in coastal areas on the western side of the Central Mountain Range surpassed 40 mm. Their findings indicated that the southwesterly airflow, carrying abundant moisture, was forced to rise upon encountering the Central Mountain Range. This led to the rapid lifting of moist air, intensifying the convective systems and subsequently enhancing precipitation intensity. In contrast to the windward slopes, the leeward slopes experienced less rainfall due to the descending motion of airflow after crossing the mountains, which reduced moisture and weakened precipitation intensity (Tai et al. 2020).

Previous studies employed two-dimensional and three-dimensional idealized numerical simulations to analyze the impact of topography on precipitation intensity and distribution under different wind speeds. The findings revealed that when low-speed moist airflow (less than 30 m s^{-1}) encounters a mountain range, precipitation on the windward slopes obviously increases. As wind speed rises, precipitation on the leeward slopes also increases (Sever and Lin 2017). Wang et al. (2022) conducted idealized cloud-resolving simulations to analyze precipitation characteristics during Taiwan's Mei-yu season under uniform southwesterly airflow conditions, excluding the effects of fronts or other disturbances. Using 64 experimental combinations, they examined the impact of varying wind directions and speeds on orographic rainfall patterns. The results indicated that when wind speeds reached at least 12.5 m s^{-1} and the moist Froude number range between 0.35 and 0.4, larger incident angles (wind directions from 210° to 285°) favored the "flow-over" phenomenon. This phenomenon mechanically lifted unstable air, generating orographic rainfall. The maximum precipitation typically occurred on the windward slopes or near ridges in the central and southern mountain regions of Taiwan, with the most intense rainfall observed when wind directions ranged from 240° to 255°.

The size of mountains or hills has a profound impact on the distribution and intensity of surface precipitation (Houze 2012). As mountain height increases, the resistance to low-level airflow becomes greater, making it more difficult for the airflow to pass over the mountain peak. This results in stronger vertical lifting effects upstream, effectively enhancing the "actual area of influence" of the mountain on the airflow. Even if the physical width of the mountain remains, the vertical lifting region extends farther upstream. This phenomenon not only increases precipitation on the windward slopes but also alters the precipitation distribution pattern. Additionally, it affects the precipitation distribution in downstream regions (Watson and Lane 2012). Previous numerical simulation studies have also demonstrated that when airflow encounters a mountain range, orographic forcing mechanically enhances upward moisture transport and the formation of hydrometeors, thereby increasing precipitation in mountainous regions (Lin 2007). Higher mountain ranges generally produce more precipitation on the windward slopes. However, beyond a certain height, some precipitation is shifted upstream. Wider mountain ranges (e.g., with a half-width of 50 km) capture more moisture on the windward slopes due to a larger uplift region, resulting in a broader precipitation area. Wide and high mountains enhance precipitation on the windward slopes, while narrow and lower mountains allow some precipitation to be transported to the leeward slopes (Colle 2004).

Additionally, variations in topographic geometry are closely related to precipitation patterns. Idealized numerical simulations have analyzed airflow motion over different ridge shapes, resulting in obvious changes in precipitation amount and distribution. For example, over a straight ridge, airflow exhibits linear motion, ascending along the ridge and crossing the peak, with precipitation primarily concentrated on the windward side and distributed relatively evenly. Over a concave ridge, airflow is guided and accelerated at the center of the ridge, leading to more concentrated precipitation near the ridge's peak. Over a convex ridge, airflow moves more smoothly, with little deceleration or concentration after crossing the peak, resulting in less leeward-side precipitation, and broader precipitation distribution, but weaker overall precipitation intensity (Watson and Lane 2012; Jiang 2006). Beyond ridge shapes, changes in wind direction obviously influence precipitation distribution, while moisture content and relative humidity have a notable impact on precipitation over concave ridges (Jiang 2006). Cornejo et al. (2024) indicated that numerical simulation results show that when Taiwan's terrain height is halved, the precipitation amount, duration, and intensity over the northern and central mountain ranges decrease obviously. This reduction is primarily attributed to the weakened orographic barrier effect, particularly as the Mei-yu front loses its enhanced orographic lifting near mountainous regions, resulting in diminished precipitation. In northern Taiwan, Datun Mountain, with its concave structure (i.e. funnel-shaped valley), promotes strong lifting of airflow as it enters the concave terrain, enhancing both the intensity and duration of precipitation (Yu et al. 2022). However, there are still relatively few studies on how topography at different locations in the same mountain range affects precipitation amount and intensity.

The Mei-yu front influenced Taiwan from May 19 to 24, 2020. Due to the front lingering near Taiwan for nearly a week, obvious rainfall occurred across western Taiwan from north to south, except for eastern regions. The primary occurrence of heavy rainfall was on the 22nd, with record-breaking precipitation observed at the Qiaotou station in southern Taiwan within just a few hours during the Mei-yu front period. Therefore, this study focuses on the extreme rainfall event of May 22nd to investigate the atmospheric environmental changes under the influence of the Mei-yu front and the role of complex topography in the heavy rainfall mechanism. The research is centered on the following three scientific questions: 1. What were the main causes of the localized heavy rainfall in southern Taiwan on the afternoon of May 22nd? 2.What environmental factors obviously influenced the development of the mesoscale convective system (MCS) over the southwestern waters of Taiwan? Was the moisture supply from the LLJ a crucial factor in the intensification of the MCS? 3.When the MCS moved over land, how did the terrain of southern Taiwan—descending from over 3,000 m to below 600 m—affect the precipitation of the MCS?

This study is divided into four main sections. The introduction reviews previous research on MCS and terrain-induced precipitation. The second section explains how the environmental atmospheric structure and southwesterly airflow influenced the intensity changes of the MCS during the southward movement of the Mei-yu front, along with a description of the simulation design used in this study. The third section discusses the simulation results, focusing on how environmental factors, such as the southwesterly airflow, affected MCS intensity changes as it formed in the Taiwan Strait and moved southeastward. It also analyzes the role of MCS and complex topography in the heavy rainfall observed in southern Taiwan. Finally, the study concludes with key findings.

2 Materials and methods

This study utilized the National Centers for Environmental Prediction (NCEP) Final Operational Global Analysis (FNL) data from 0000 UTC on May 21 to 0000 UTC on May 24, 2020, with a temporal resolution of six hours (13 datasets in total) and a spatial resolution of 0.25°. These data come from the Global Data Assimilation System (GDAS), which continuously gathers observational data from the Global Telecommunications System (GTS) and other sources for multiple analyses. FNL data not only includes surface data but also provides atmospheric variables at multiple pressure levels, typically covering up to 26 levels between 1000 hPa and 10 hPa. The available variables include temperature, wind speed, wind direction, geopotential height, relative humidity, and specific humidity (NCEP, 2015). Additionally, data from the Atmospheric Science Research and Application Databank (ASRAD) supported by Chinese Culture University, as well as resources from the National Science and Technology Center for Disaster Reduction (NCDR) and the Central Weather Administration (CWA) of Taiwan, were employed. These include surface weather charts, satellite images, skew-T diagrams, visible and infrared satellite imagery, radar reflectivity, and surface observation data to conduct both observational and simulation-based analyses.

ASCAT (Advanced Scatterometer) is an active microwave radar scatterometer installed on meteorological satellites to measure ocean surface wind fields (wind speed and direction). It operates by emitting microwave signals and receiving the scattered signals reflected from the ocean surface. By analyzing the wave patterns, ASCAT estimates wind field information. ASCAT data is widely used in weather forecasting, oceanographic research, and the initialization and validation of numerical weather prediction models (Hersbach and Stoffelen 2000; Verhoef et al. 2022).

2.1 Synoptic Environmental Analysis

On May 22, 2020, the Special Sensor Microwave Imager/Sounder (SSMI/S) onboard the F18 satellite (Fig. 1) revealed a high-moisture region extending from the South China Sea across Taiwan, the Ryukyu Islands, and the southern seas of Japan, almost reaching the western coast of the United States. This pattern resembles an "atmospheric river" transporting moisture. Chien and Chiu (2023) found that in May 2020, a stronger Pacific subtropical high and southwesterly monsoon airflow intensified the moisture transport belt over northern Indochina. Their research shows when the eastern portion of the SWV touched northern Taiwan, its associated west-southwesterly winds and the largescale southwesterly monsoonal flow transported moisture toward the Taiwan Strait. The moisture-laden southwesterly flow was lifted by the stationary Mei-yu front, leading to the heavy rainfall in southern Taiwan. When the SWV passed through northern Taiwan, it became the dominant weather system that enhanced the west-southwesterly winds and transported moisture from South China to Taiwan. On May 21 and 22, as the SWV passed over northern Taiwan, it enhanced the southwesterly winds, transporting moisture from southern China to Taiwan.

On May 22, 2020, the East Asian surface weather chart at 0800 LST (0000 UTC) (Fig. 2a) showed a stationary front extending southwestward from the center of an extratropical cyclone over the central North Pacific (not shown), passing through the seas near the Ryukyu Islands and the seas adjacent to northern Taiwan, and terminating at a localized low-pressure center near Hainan Island. Convective cloud systems were forming near the Ryukyu Islands. At the same

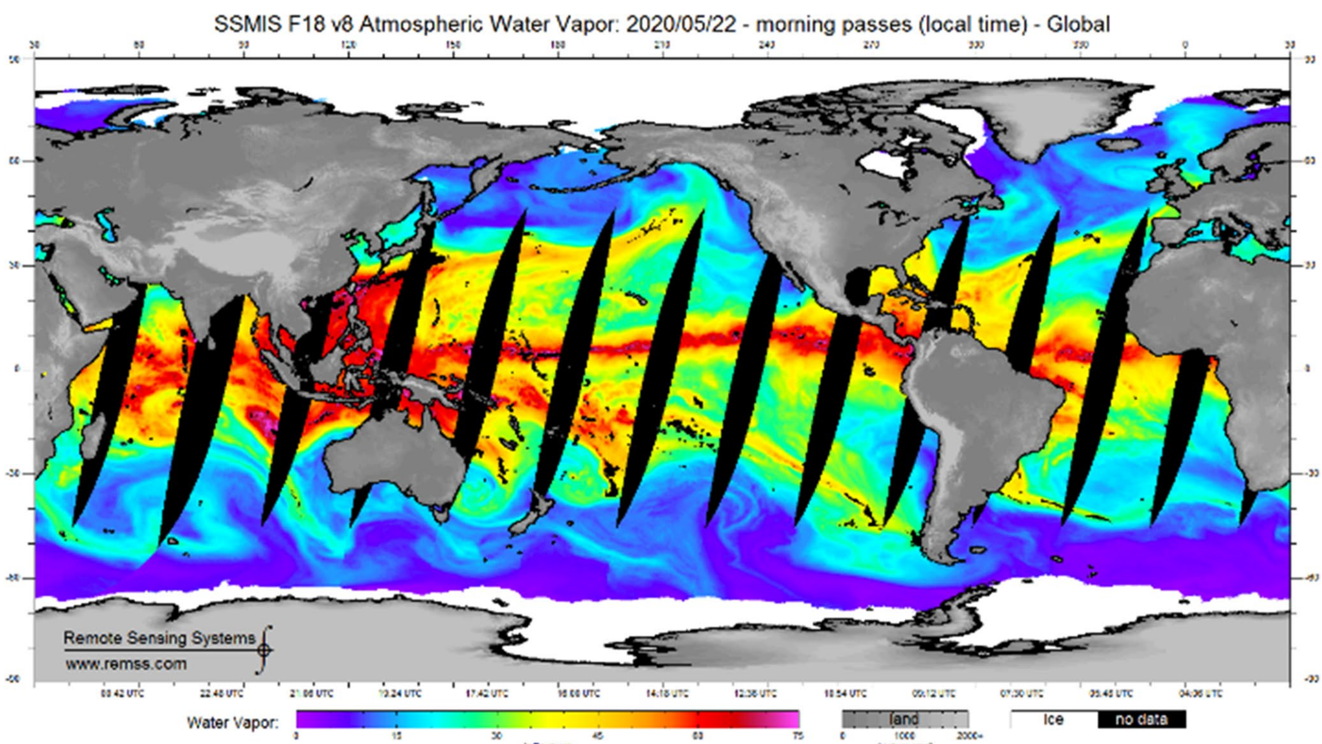

Fig. 1 During the morning hours of May 22, the atmospheric water vapor microwave remote sensing observation image from the SSMI/S onboard the F18 satellite (unit: mm). Atmospheric water vapor content corresponds to the color bar below

time, MCSs exhibited enhanced convective activity and cloud growth from the northern Taiwan Strait to areas near Hong Kong and Hainan Island. This pattern is evident in the reanalysis field shown in Fig. 2b, where, at the same time, a large area with equivalent potential temperature exceeding 351 K at 850 hPa covered regions surrounding Taiwan, as well as areas from Hong Kong to Hainan Island. This area roughly corresponds to the regions where MCSs were actively developing. During this period, the southwesterly winds were already strong, exceeding 10 m s^{-1}. The reanalysis data of moisture flux (Fig. 2c) reveal that the strongest moisture flux occurred over the seas near the Ryukyu Islands, the seas adjacent to northern Taiwan, and areas near Hainan Island, providing abundant moisture to support convective development. At 500 hPa, the eastward movement of the trough increased positive vorticity (Fig. 2d). Combined with upper-level divergence at 200 hPa (Fig. 2e), this strengthened the dynamic development mechanisms of MCSs. The combination of low-level convergence and upper-level divergence in the atmospheric dynamical field created favorable conditions for the development of convective systems.

2.2 Regional Observational Data Analysis

At 0100 LST on May 22, radar reflectivity images revealed a northeast-southwest oriented MCS over the offshore waters of southwestern Taiwan (Fig. 3a). By 0200 LST (Fig. 3b), the MCS had developed further, becoming more organized and gradually moving southeastward onto Taiwan. By 0300 LST (Fig. 3c), the right side of the MCS had visibly weakened due to interaction with Taiwan's complex terrain, which reduced its intensity through precipitation. Overall, the appearance of the MCS resembled the characteristics of a bow echo associated with a squall line. By 1400 LST (Fig. 3d), the MCS reappeared, with the strong reflectivity area of the linear convective system becoming broader. At this time, the mountainous regions of southwestern Taiwan appeared to be influenced by the lifting effect of the Mei-yu front and thermal convection, leading to an increase in reflectivity intensity. One hour later (Fig. 3e), the MCS merged with the pre-existing thermal convective cells developing in the southwestern mountainous regions, forming a northeast-southwest oriented linear convective system that continued to intensify. By 1600 LST (Fig. 3f), the MCS moved slowly southeastward, but it maintained its linear convective structure. Additionally, a secondary strong reflectivity area extended from the offshore seas of southwestern Taiwan to the southwestern mountainous regions. Heavy rainfall persisted over both the plains and mountainous regions of southwestern Taiwan.

To understand the dynamical and thermodynamic characteristics of the southwesterly airflow, sounding data from Pratas Island, Penghu Airport, and Pingtung Airport (Fig. 4) were analyzed. The skew-T diagram from Pratas Island (Fig. 5a) at 0800 LST on May 22 shows that the environmental wind field featured southwesterly winds in the lower levels, gradually veering clockwise with height, becoming westerly at 500 hPa. This indicates obvious warm advection in the mid-to-lower troposphere. The mean wind speed from near the surface to 700 hPa ranged from 30 to 40 KTS (15.4 m s^{-1} to 20.6 m s^{-1}), meeting the criteria for a LLJ over the ocean. Additionally, the convective available potential energy (CAPE) reached a maximum of 3897 m^2 s^2. The lifted condensation level (LCL) was only around 122 m, and the level of free convection (LFC) was approximately 1.116 km, providing favorable conditions for system development. Thermodynamic indices, including the K index, Total index, and Showalter index, indicated that the atmosphere over the offshore area of southwestern Taiwan was highly unstable. The skew-T diagram for the Penghu (Fig. 5b) at 0800 LST (0000 UTC) on the same day shows weak northeasterly winds near the surface at the leading edge of the Mei-yu front. With increasing altitude, the wind direction veered from south-southwesterly to southwesterly. The overall environmental wind field also exhibited obvious warm advection. The wind speed between 850 and 700 hPa ranged from 20 to 25 KTS (10.3 m s^{-1} to 12.9 m s^{-1}), meeting the criteria for a LLJ. No obvious CAPE was observed, and the LCL was approximately 133 m. Thermodynamic indices were similar to those at Pratas Island, indicating that the atmosphere was highly unstable. Relative humidity below 700 hPa was notably high. These findings suggest that the central Taiwan Strait was simultaneously influenced by abundant moisture transport from the southwesterly airflow and the lifting effect of the gradually southward-moving leading edge of the Mei-yu front, creating favorable conditions for the development of maritime convection.

The skew-T diagram from Pingtung Airport in southwestern Taiwan at 0800 LST on the same day (Fig. 6a) reveals that only the lowest level was affected by localized terrain, exhibiting weak northeasterly winds. Below 700 hPa, however, the southwesterly winds were strong (exceeding 30 KTS, i.e., exceeding 15.4 m s^{-1}), indicating the presence of a LLJ. The environmental wind field also showed warm advection with a clockwise veering of wind direction with height. Notably, the LCL was only about 67 m, and the convective condensation level (CCL) was approximately 714 m. This indicates that only a slight lifting was required for cloud formation. Especially with abundant moisture, the release of latent heat during lifting accelerated the development of the convective system. By 2000 LST (Fig. 6b), the LCL at Pingtung Airport slightly increased to 70 m, but

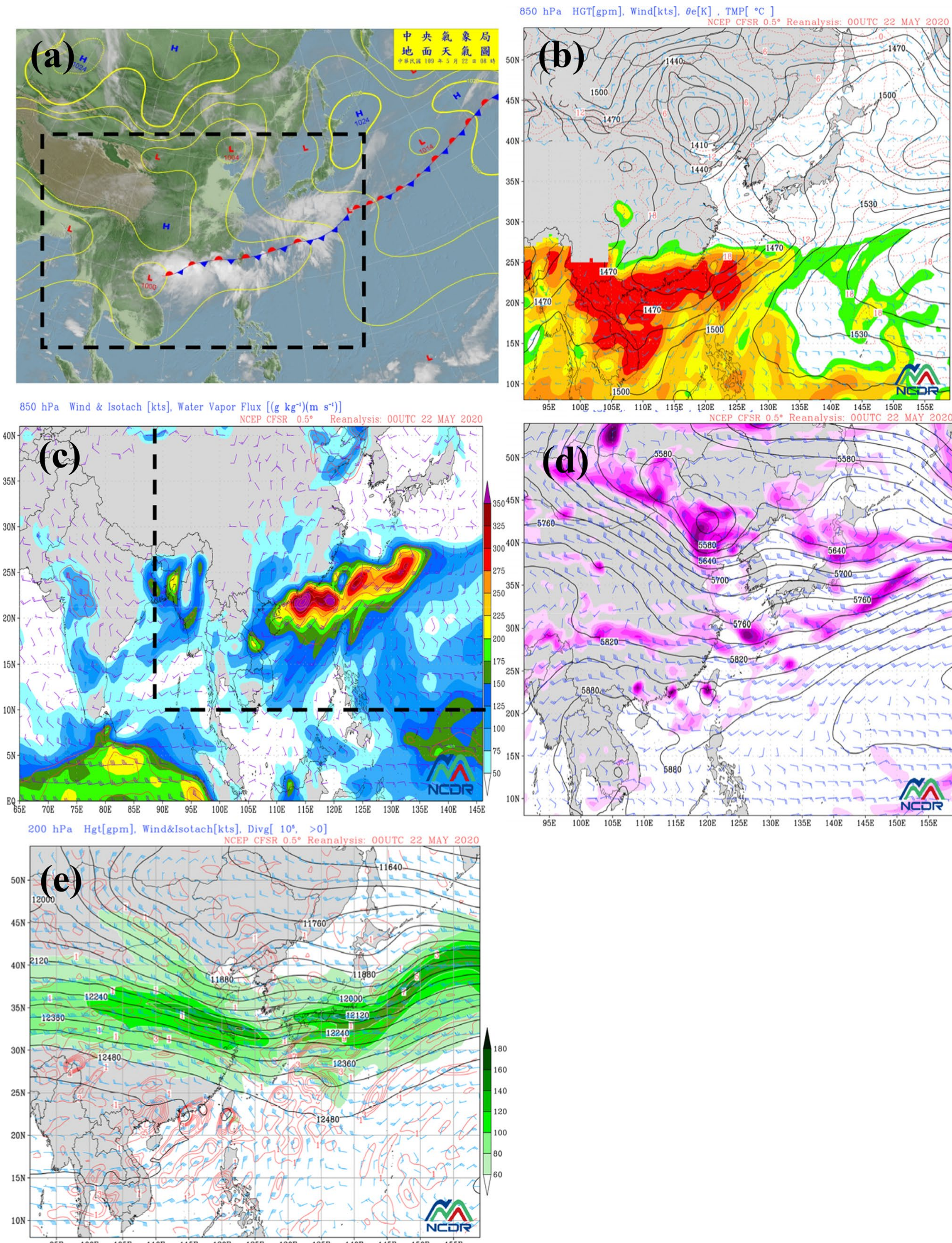
(a)
中央氣象局
地面天氣圖
850 hPa HGT[gpm], Wind[kts], θe[K], TMP[°C]
NCEP CFSR 0.5° Reanalysis: 00UTC 22 MAY 2020
(b)
850 hPa Wind & Isotach [kts], Water Vapor Flux [(g kg⁻¹)(m s⁻¹)]
NCEP CFSR 0.5° Reanalysis: 00UTC 22 MAY 2020
(c)
NCEP CFSR 0.5° Reanalysis: 00UTC 22 MAY 2020
(d)
200 hPa Hgt[gpm], Wind&Isotach[kts], Divg[10⁵, >0]
NCEP CFSR 0.5° Reanalysis: 00UTC 22 MAY 2020
(e)
NCDR

Fig. 2 Synoptic analysis from CWA and NCDR at 0800 LST (0000UTC) on May 22, 2020. **a** surface weather chart from CWA, **b** 850 hPa equivalent potential temperature (K) from NCDR, **c** 850 hPa moisture flux ((g kg^{-1}) (m s^{-1})) from NCDR, **d** 500 hPa vorticity (s^{-1}) from NCDR. **e** 200 hPa divergence(s^{-1}) from NCDR. The areas of images (b), (d), and (e) are indicated with black dashed lines in images (a) and (b)

the CCL dropped to 40 m, and the LFC was as low as 70 m. A lower LFC indicates that air parcels required minimal external forcing to reach the level of free convection, creating favorable conditions for the development of convective systems. Combined with the analysis of various thermodynamic indices, the results indicated that the atmosphere was in a state of "extreme instability, with potential for thunderstorms." Based on the vertical wind field analysis, compared with Pingtung Airport in southwestern Taiwan and Penghu Airport in the Taiwan Strait, where the peak wind speeds in the atmospheric boundary layer were observed between 850 hPa and 700 hPa at approximately 35 KTS (18 m s^{-1}), Pratas Island showed a similar LLJ occurrence at 850–700 hPa but with the peak wind speed observed at 925 hPa, reaching as high as 40 KTS (20.6 m s^{-1}). This indicates that the LLJ over the South China Sea was stronger and extended through a deeper layer compared to the LLJ in the adjacent and surrounding seas of Taiwan. This phenomenon was consistent with the concept of "Marine Boundary Layer Jets (MBLJ)" proposed by Tu et al. (2019). These LLJs were a critical factor contributing to the development of the MCS and the heavy rainfall in southwestern Taiwan during this event.

Additionally, color enhanced infrared satellite imagery reveals that the convective cloud systems at 0210 LST (Fig. 7a) and 1410 LST (Fig. 7b) on May 22 both exhibited characteristics of linear convection (as shown in Fig. 3a-f), with similar cloud-top heights. However, the afternoon convective cloud system was more fully developed, with cloud-top temperatures below −52 °C extending from the seas near southwestern Taiwan to the southwestern mountainous regions. Real-time lightning signals from the CWA revealed distinct differences between the early morning and afternoon periods. During the early morning (Fig. 8a), lightning strikes were few and confined to a small area in southwestern Taiwan. By the afternoon (Fig. 8b), the frequency of lightning strikes increased obviously, extending from the offshore region of southwestern Taiwan to the southwestern mountainous areas, showing a marked difference from the early morning distribution. Precipitation patterns also differed between the two periods. In the early morning (Fig. 8c), areas with rainfall exceeding 20 mm hr^{-1} were slightly larger than in the afternoon (Fig. 8d) but were distributed more unevenly. In contrast, afternoon precipitation was influenced by the intensity of convective cloud systems, with concentrated rainfall patterns and maximum hourly precipitation exceeding 80 mm hr^{-1}.

To understand the differences in MCS development before and after the frontal position at different times, we overlaid radar reflectivity images, color enhanced infrared satellite imagery, and 1000 hPa reanalysis fields for the early morning and afternoon periods (Fig. 9a and b). The analysis shows that in the frontal leading region (south of the dark blue dotted line), the reflectivity was more concentrated, with echoes continuously moving inland from the offshore area of southwestern Taiwan. The cloud-top heights were higher, with lower temperatures, and areas of stronger reflectivity were concentrated on the northern and northeastern sides of the convective cells observed in the satellite imagery. Behind the front (north of the dotted line), the reflectivity was weaker and more scattered, with most stronger echoes located along the coastal areas of central and northern Taiwan. The cloud systems were predominantly stratiform, with lower development heights. From the observations above, we concluded that the pre-frontal environment featured stronger mid- to upper-tropospheric winds and obvious vertical wind shear in the mid-to-lower layers, along with the presence of LLJs. These conditions contributed to a more unstable atmosphere with higher CAPE, allowing for deeper convective development within the system. In contrast, the post-frontal environment was characterized by drier and cooler low levels of air, resulting in lower instability and CAPE, which limited the depth of convection within the system.

From the observation data above, it can be seen that when the moist and strong southwesterly airflow was lifted by the leading edge of the Mei-yu front, MCSs formed and rapidly developed over the ocean. In the afternoon, these systems developed even more quickly than in the early morning. This is consistent with the findings of Chen (1992), which indicate that the convergence of the Mei-yu front and low-level jet results in the rapid development of MCSs due to the uplift of abundant moisture and the subsequent release of latent heat. As the MCSs moved eastward from the offshore areas of Taiwan to its landmass, the complex terrain in southwestern Taiwan further enhanced convective precipitation, ultimately leading to heavy rainfall in the region.

2.3 Model Configuration and Experimental Design

This study employed the Weather Research and Forecasting (WRF) Model V4.2.1 to simulate the surrounding regions of Taiwan from 1200 UTC (2000 LST) on May 20 to 1800 UTC (0200 LST on May 24), 2020. A two-layer nested grid configuration was used (Fig. 10), with the highest

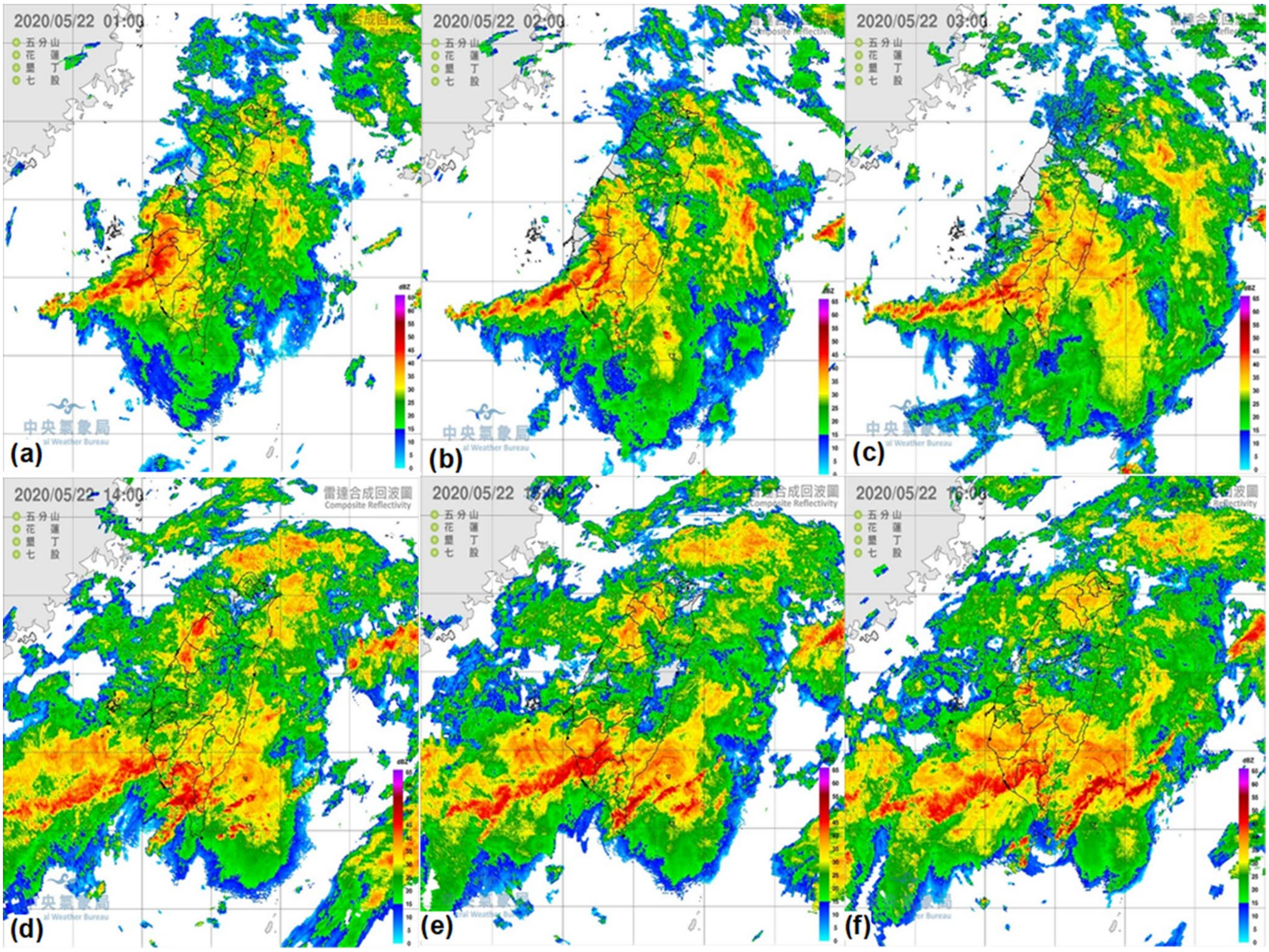

Fig. 3 Composite reflectivity images of weather radar on May 22, 2020 from CWA. **a** 0100 LST, **b** 0200 LST, **c** 0300 LST, **d** 1400 LST, **e** 1500 LST, **f** 1600 LST

spatial resolution of 2 km. The initial and boundary conditions were derived from the reanalysis data provided by the NCEP, with a 6-hour interval. The parameterization schemes in WRF were listed as follows: the WRF Single Moment 5 class (WSM5) scheme (Hong et al. 2004) used for the cloud microphysics process, the MM5 scheme (Beljaars 1995) used for the surface layer process, the Yonsei University scheme (YSU) (Hong et al. 2006) used for the boundary layer process, the Rapid Radiative Transfer Model (RRTM) longwave radiation scheme (Mlawer et al. 1997), the Goddard Shortwave scheme (Chou and Suarez 1999) for the short −wave radiation, and the Kain-Fritsch (KF) scheme(Kain 2004) for the cumulus cloud parameterization in domain 01. D02 does not use cumulus parameterization.

3 Results and Discussion

3.1 The Impact of Southwest Airflow on Moisture Transport and Precipitation

Through satellite observations (Fig. 11a) and the wind field simulated by the WRF model (Fig. 11b), it can be seen that the southwesterly flow over the offshore area of southwestern Taiwan is quite strong (highlighted by the red box in Fig. 11). Meanwhile, a wind discontinuity zone caused by the Mei-Yu front is present in the central Taiwan Strait. In this case, the wind speed simulated by the WRF model is slightly higher than the 10-meter ocean surface wind observed by the satellite-based ASCAT (The Advanced Scatterometer), while the wind direction is quite similar.

This case of stronger southwesterly airflow was caused by the monsoon circulation and the eastward movement of a SWV (Chien 2015). The enhanced southwesterly airflow, accompanied by an LLJ carrying abundant moisture,

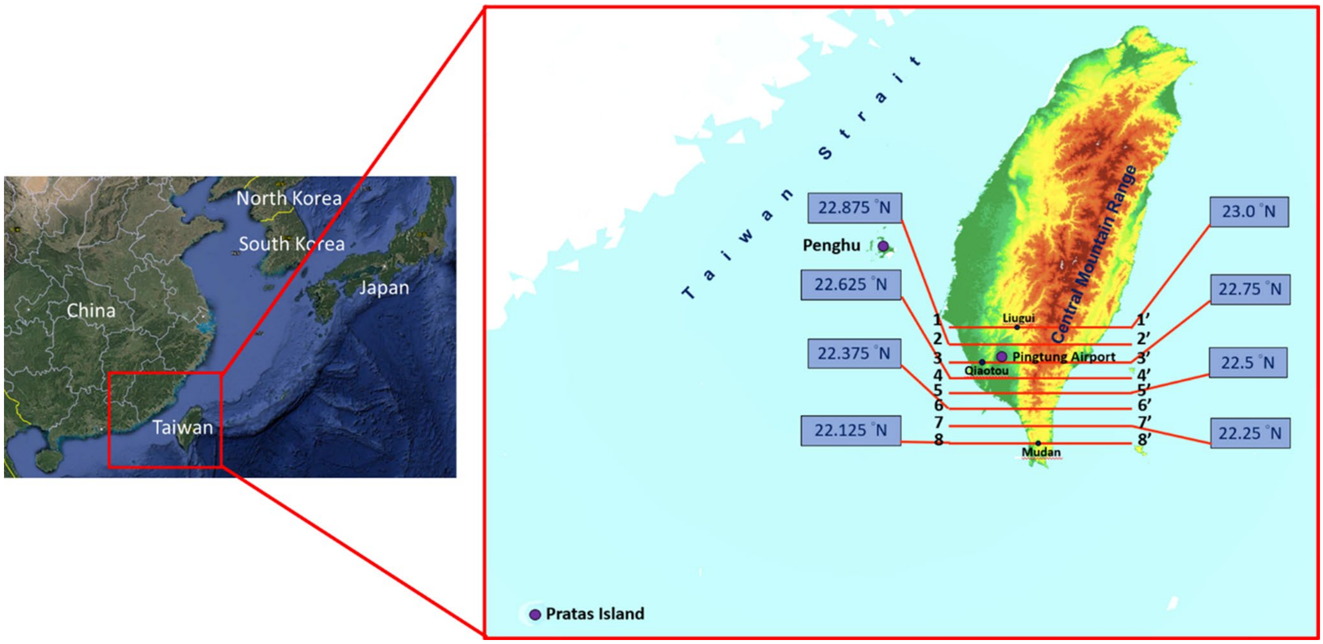

Fig. 4 Enlarged schematic map of a partial region in Southeast Asia, showing the locations of Pratas Island, Penghu, Pingtung Airport, and vertical cross-section positions over the southern Central Mountain Range of Taiwan. The cross-sections range from 11' to 88', corresponding to 23°N to 22.125°N, with an interval of 0.125° (approximately 13.8 km), resulting in a total of 8 vertical cross-sections

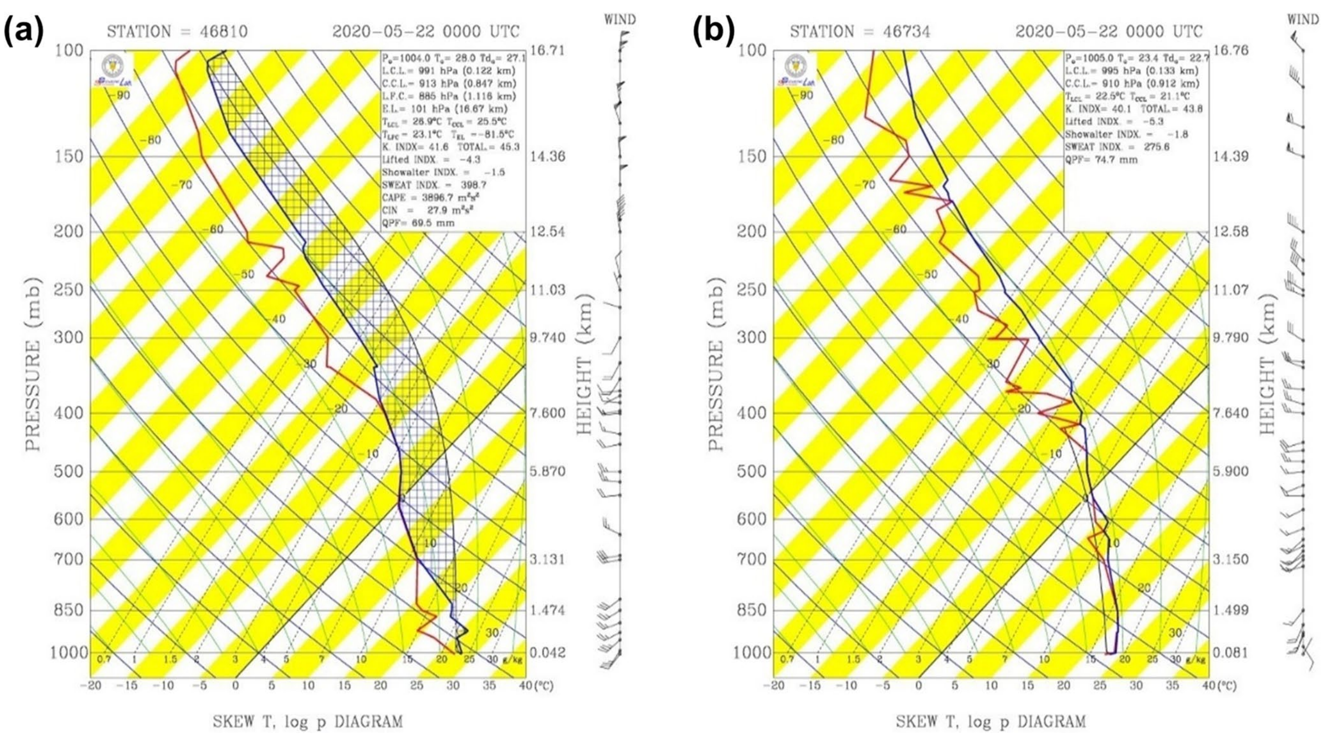

Fig. 5 Skew-T diagrams at 0800 LST on May 22, 2020, **a** Pratas Island and **b** Penghu from CWA

led to the formation of MCSs in the southwestern Taiwan Strait. These MCSs not only developed rapidly but also contained vigorous convective cells often associated with lightning activity. Analyzing the simulation results at 1200 LST on May 22 (Fig. 12a), the MCS at this time differed from the linear convective systems observed during the early morning and afternoon periods. Although it lacked a specific organizational pattern, it covered a broader area, with numerous convective cells producing strong reflectivity within the MCS. The hourly rainfall maps reveal

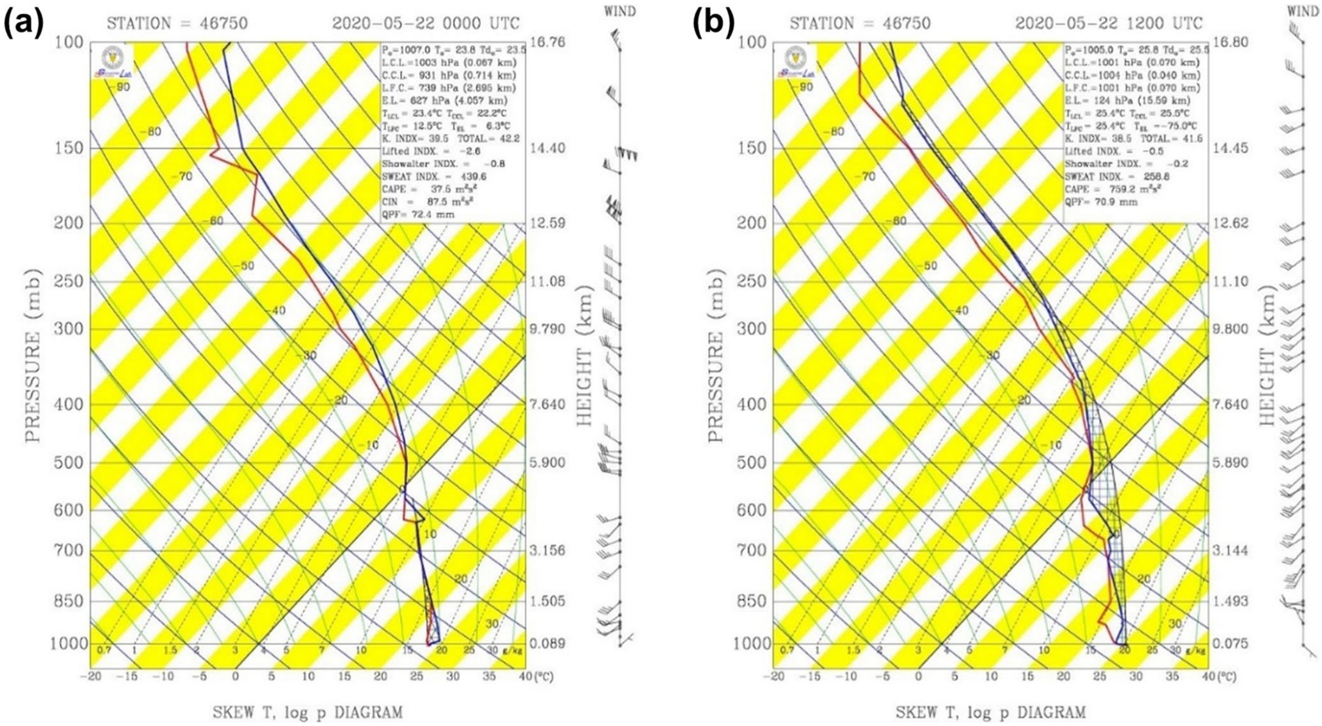

Fig. 6 Same as the figure 5, but at Pingtung Airport at (**a**) 0800 LST and (**b**) 2000 LST from CWA

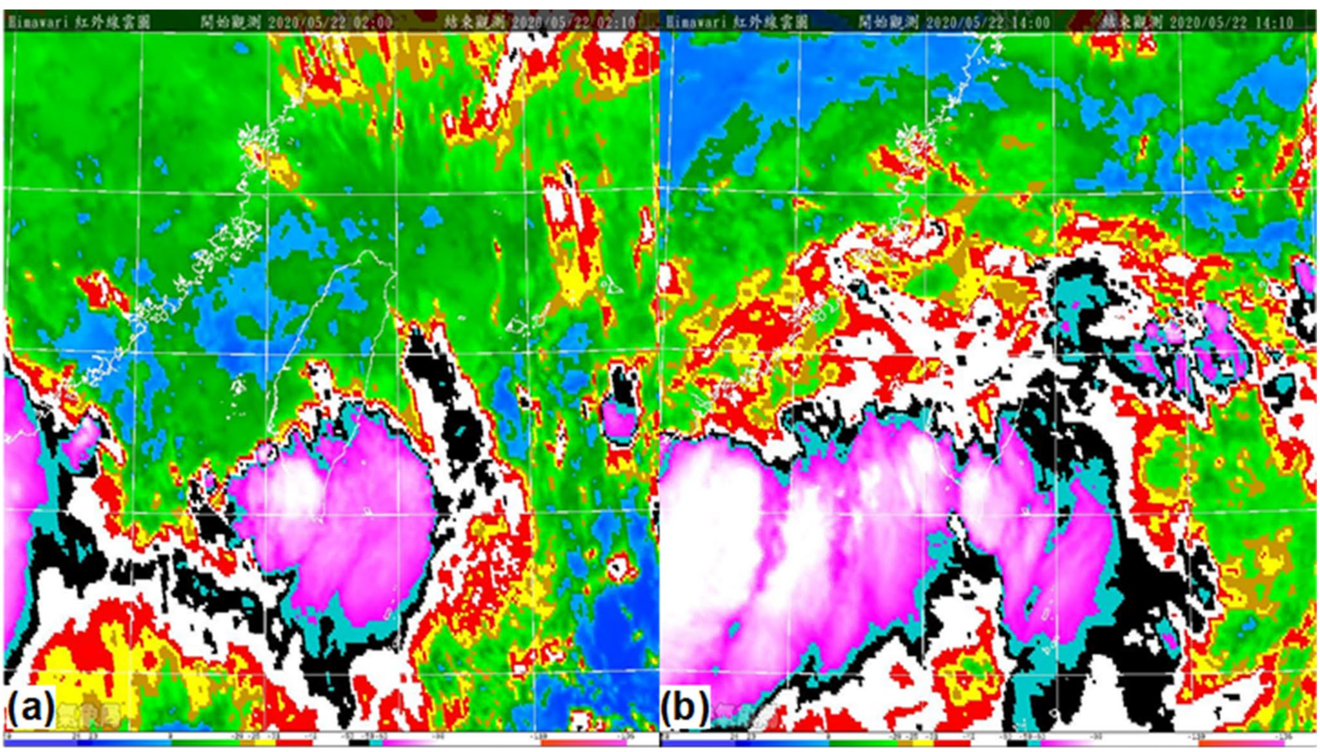

Fig. 7 Color enhanced infrared satellite imagery around Taiwan on May 22, 2020 from CWA: **a** 0210 LST; **b** 1710 LST

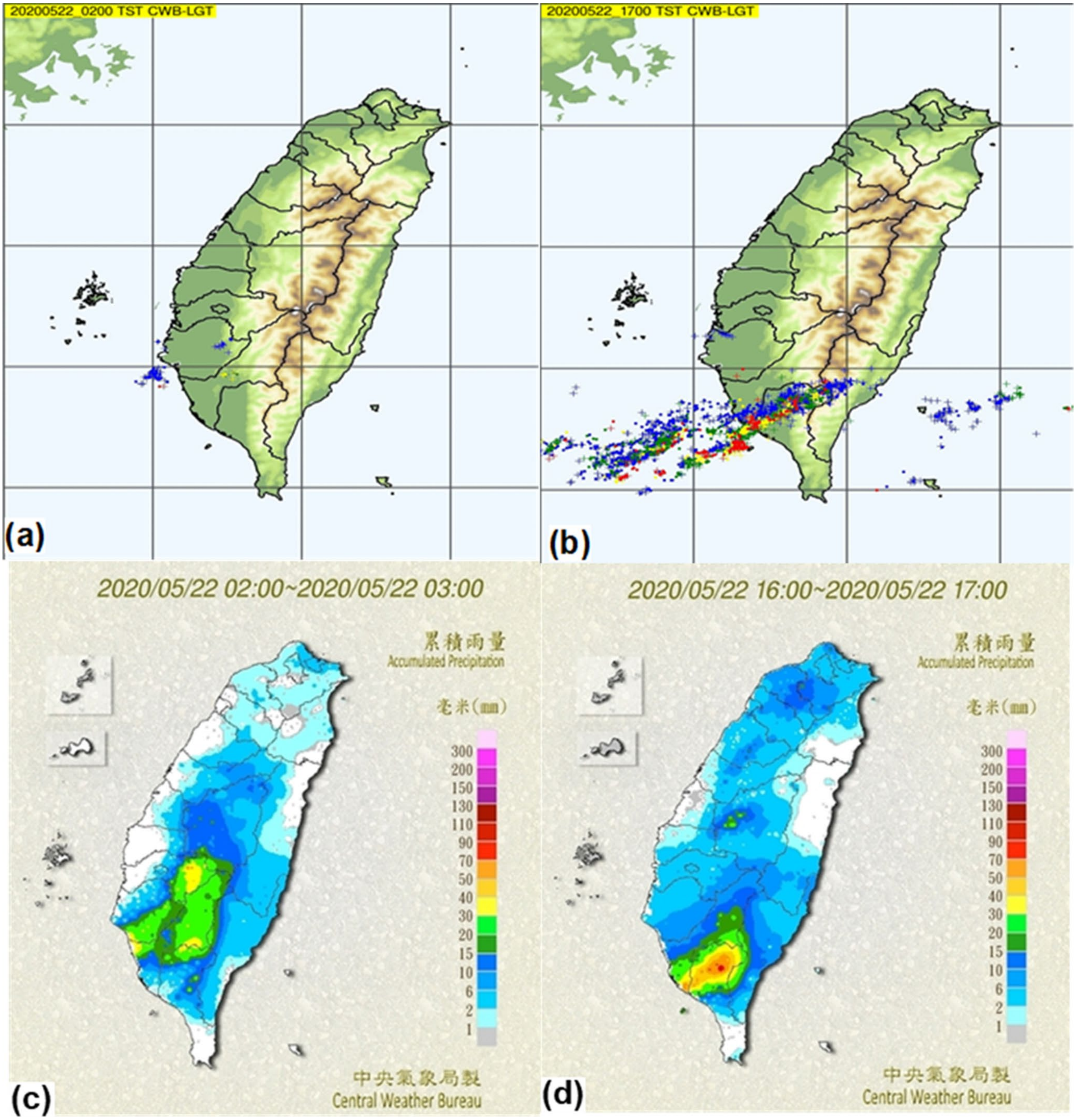

Fig. 8 Lightning observation and hourly rainfall maps for Taiwan on May 22, 2020 from CWA: **a** and **b** show lightning observations at 0200 LST and 1700 LST, respectively, with red representing lightning strikes within the past 0–5 minutes, yellow for 5–10 minutes, green for 10–30 minutes, and blue for 30–60 minutes. **c** and **d** show hourly rainfall maps for 0200–0300 LST and 1600–1700 LST, respectively. The color bar on the right indicates accumulated rainfall (mm)

that precipitation associated with the MCS was concentrated over the offshore areas of southwestern Taiwan and the southwestern land regions, with the heaviest and most focused rainfall occurring in the southwestern mountainous areas (Fig. 12b). The moisture supply for the MCS was primarily transported by the 850 hPa LLJ (Fig. 12c), which drove moisture convergence along the leading edge of the front (Fig. 12d). This moisture convergence, accompanied by the release of latent heat from convection, heated the atmosphere and lowered local pressure. Due to the convergence of a large amount of moisture and the release of latent heat, the trough line usually deepens, and vorticity

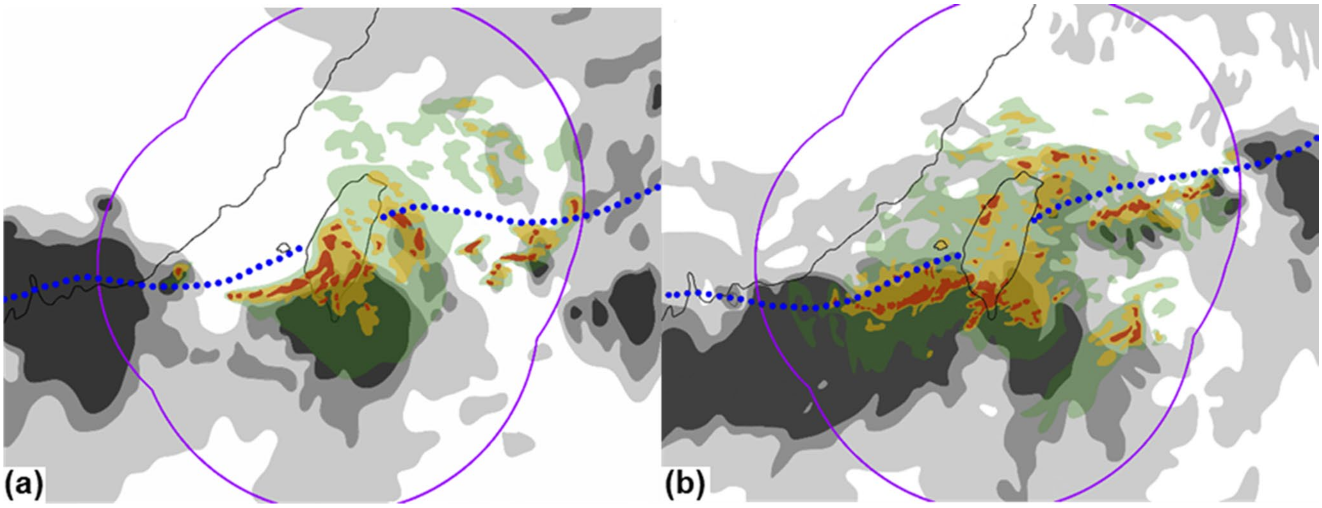

Fig. 9 Overlay schematic diagrams combining radar reflectivity, color enhanced infrared satellite imagery, and 1000 hPa reanalysis fields. **a** 0200 LST on May 22, **b** 1400 LST on May 22. The dotted dark blue line indicates the discontinuity in wind direction. The thick purple solid line represents the radar scan area. The gray shading indicates cloud-top temperatures: dark (≤-63°C), medium (-53°C to -63°C), and light (-25°C to -53°C). The colored scale represents radar reflectivity, red (>40 dBZ), yellow (>30 dBZ), and green (>15 dBZ)

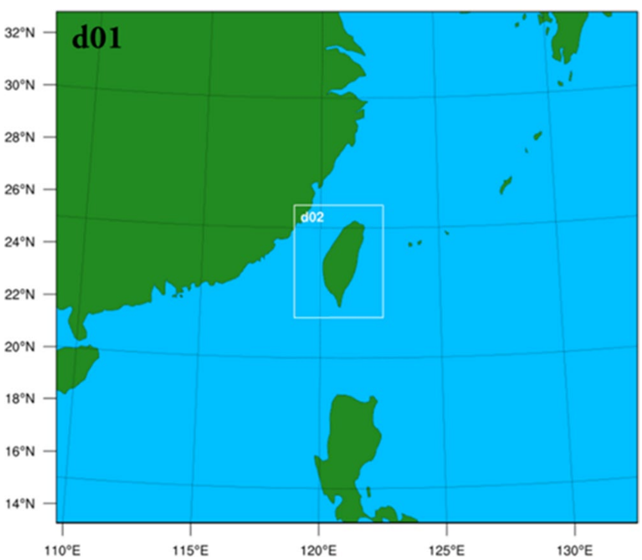

Fig. 10 Domain setting of the model, including two nested domains with 10 and 2 km horizontal space resolutions

increases (Fig. 12e). The enhanced pressure gradient alters the local wind field, strengthening the maximum wind speed at the center of the LLJ, which in turn induces stronger low-level convergence. At this time, coupled with the divergence effect of the upper-level diffluent flow field (Fig. 12f), the development of the MCS is further intensified, enhancing its strength and sustaining its formation.

Using Fig. 11, the red box represents the source region of the southwesterly flow affecting southern Taiwan. The grid data within this region is averaged from 0500 to 1300 UTC to quantify the moisture supply from the southwesterly flow and analyze the impact of environmental variables in this area on the intensity variations of the MCS near southern Taiwan. From the figure, it can be observed that over the ocean, due to the lack of topographic barriers or lifting effects, the intensity of MCS is primarily determined by dynamic conditions such as wind field convergence and divergence, vertical motion, as well as thermodynamic factors including moisture supply and phase transitions, which influence the strength of MCS radar echoes. From Table 1, it can be seen that low-level wind field convergence, moisture supply, and the amount of rainwater resulting from the massive release of latent heat through condensation have the greatest impact on MCS radar echoes. Other factors show relatively lower correlation coefficients when averaged. This indicates that in the southwestern waters of Taiwan, during the period from 0500 to 1300 UTC, the moisture provided by the southwesterly flow through the LLJ, along with low-level wind field convergence and moisture processes, are the key factors influencing MCS intensity variations. In other words, changes in the environmental field are closely related to the rapid development of the MCS system itself.

3.2 The Mechanism of Complex Terrain Affecting Precipitation

During the heavy rainfall over Taiwan on May 22, the observed (Fig. 13a) and simulated (Fig. 13b) precipitation distribution patterns were generally consistent. Using Chiayi City (23.5°N) as a dividing line, the simulated total rainfall in areas north of Chiayi, particularly in northwestern Taiwan, was lower than the observed values. South of Chiayi, the simulations captured areas with higher rainfall along the coast, which continued to extend inland toward

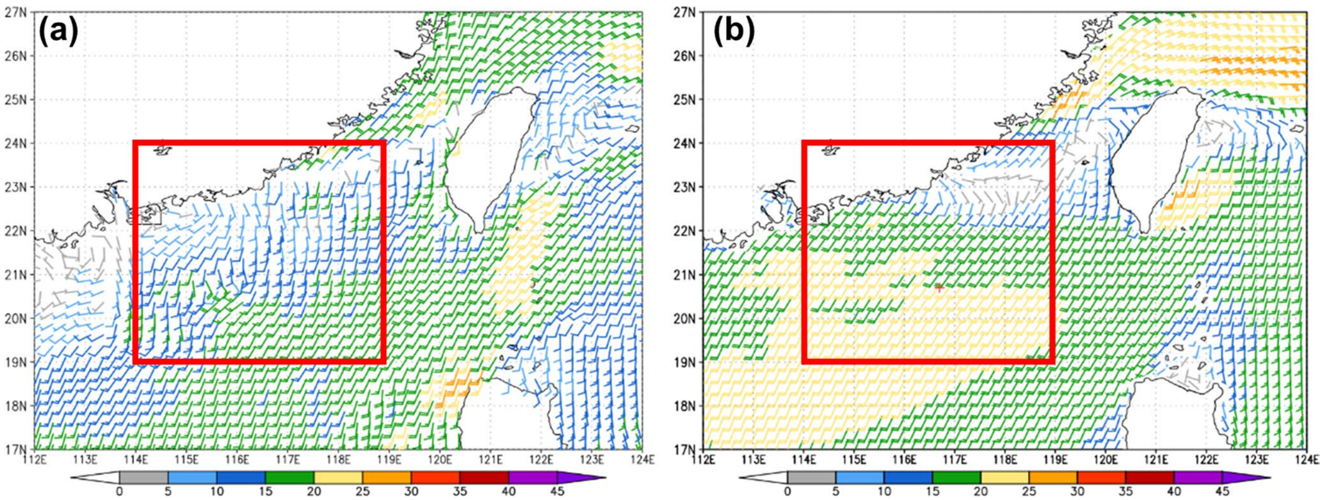

Fig. 11 Comparison of wind fields over the offshore area of southwestern Taiwan at 0800 LST on May 22. **a** observed 10-m wind from satellite data; **b** simulated 10-m wind field. The color shading corresponds to wind speed (KT) as indicated by the color bar below. The red box represents the selected area for grid-averaged analysis (114°–120°E, 19°–24°N)

the mountainous regions. Overall, the daily accumulated rainfall distribution from the simulation shows that in areas north of Chiayi, rainfall increased continuously from the coastline inland, with the highest accumulation observed in the mountainous regions. The area south of Chiayi has a much larger area of heavy rainfall than the area north of Chiayi. This indicates that as the Mei-yu front oscillated north and south over Taiwan, the MCS caused two distinct types of rainfall in areas north and south of Chiayi. Although Chiayi served as the dividing line for these different rainfall patterns, both regions exhibited maximum rainfall in the mountainous areas, highlighting the role of Taiwan's complex terrain in enhancing regional precipitation.

To understand the reasons for changes in convective intensity when an MCS moves from the ocean to land, we analyzed the radar reflectivity, vertical motion, and wind field in Qiaotou District, Kaohsiung City (22.75°N) during the heavy rainfall period in the afternoon (1300–1800 LST) using a time series of vertical atmospheric cross-sections (Fig. 13b). The results show that the MCS had already begun to intensify over the ocean (Fig. 14a). In Fig. 14a, the intensification of the MCS is accompanied by changes in the low-level wind field over the ocean, particularly when the southwesterly flow and northwesterly wind converge, creating optimal low-level moisture convergence and uplift. As a result, convection cells developed rapidly over the ocean and have produced heavy precipitation. At this time on land, there are southwest to south-southwesterly winds in the low-level wind field, and convective cells begin to strengthen due to low-level convergence. Over the mountainous region, where the terrain is steep, the lifting effect further accelerates the intensification of convective cells, making them strengthen more rapidly than those in the land area ahead (left side of the figure). The environmental wind field, influenced by the terrain, transitions from southwesterly to west-southwesterly. In the area behind the mountains, terrain effects suppress the occurrence of convective cells. The environmental wind field here is south-southwesterly, with only scattered rainfall, which contrasts with the situation in the area ahead of the mountains.

After one hour of development and precipitation (Fig. 14b), the MCS slightly weakened in intensity. However, overall, a similar pattern to Fig. 14a emerged, where convective cells developed more strongly over the ocean and in front of the mountainous region, while those behind the mountains were weaker. Although the precipitation at this time was not as intense as in Fig. 14a, it was still influenced by the terrain effect, with rainfall concentrated in front of the mountainous region. By 1500 LST (Fig. 14c), the MCS had strengthened again, with convective cells rapidly developing over the ocean and in front of the mountains. The precipitation corresponded to the development of convective cells and the influence of the terrain effect, remaining concentrated in front of the mountainous region. Notably, due to the highly unstable environmental atmosphere at this time, scattered convection was present behind the mountains. However, the low-level environmental wind field behind the mountains remained from the south-southwest and was not affected by the development of convective cells. In Fig. 14d and f, it can be observed that the MCS continues to develop, with its convective cells gradually moving from the windward side to the leeward side (west to east). Although some convective cells appear to cross the mountainous region, their convection weakens rapidly. Notably, precipitation is almost entirely intercepted by the terrain, resulting in obviously lower rainfall on the leeward side compared to the

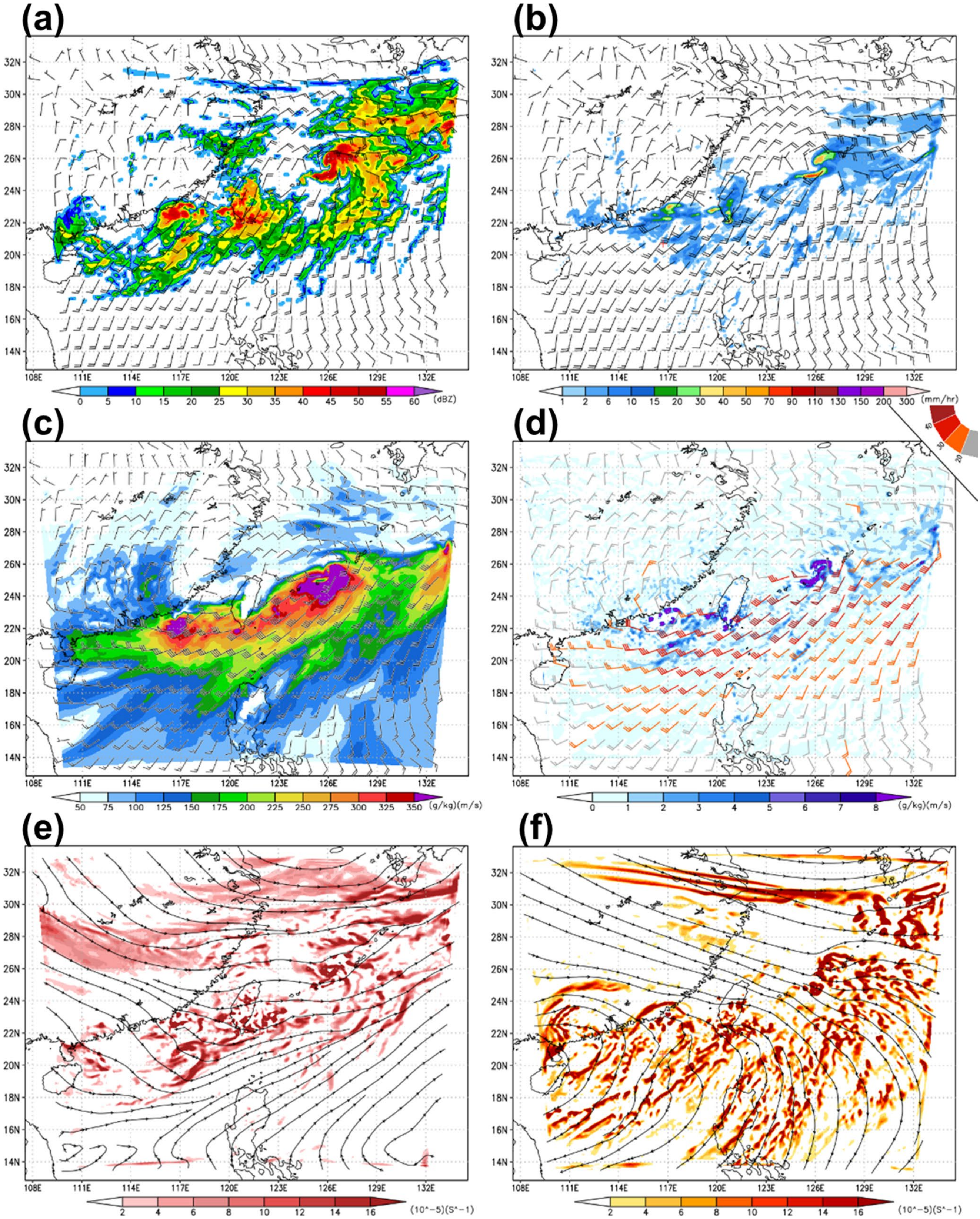

Fig. 12 At 1200 LST on May 22, 2020. **a** radar reflectivity and 10-m wind field, **b** one-hour accumulated rainfall and 10-m wind field, **c** 850 hPa moisture flux and wind field, **d** convergence and 850 hPa wind field, **e** 500 hPa vorticity, **f** 200 hPa divergence and streamline simulation. The colors in each figure correspond to the color bar shown below

Table 1 Correlation coefficients of various meteorological variables between radar echo intensity and simulation

Variable 1	Radar echo intensity (1300–2100 LST)					
Variable 2	Low level wind Convergence (1000 − 500 hpa)	High level wind divergence (400–200 hpa)	Vertical velocity	Water vapor	Cloud water	Rain water
Correlation Coefficient	0.862	0.365	0.351	0.930	0.420	0.896

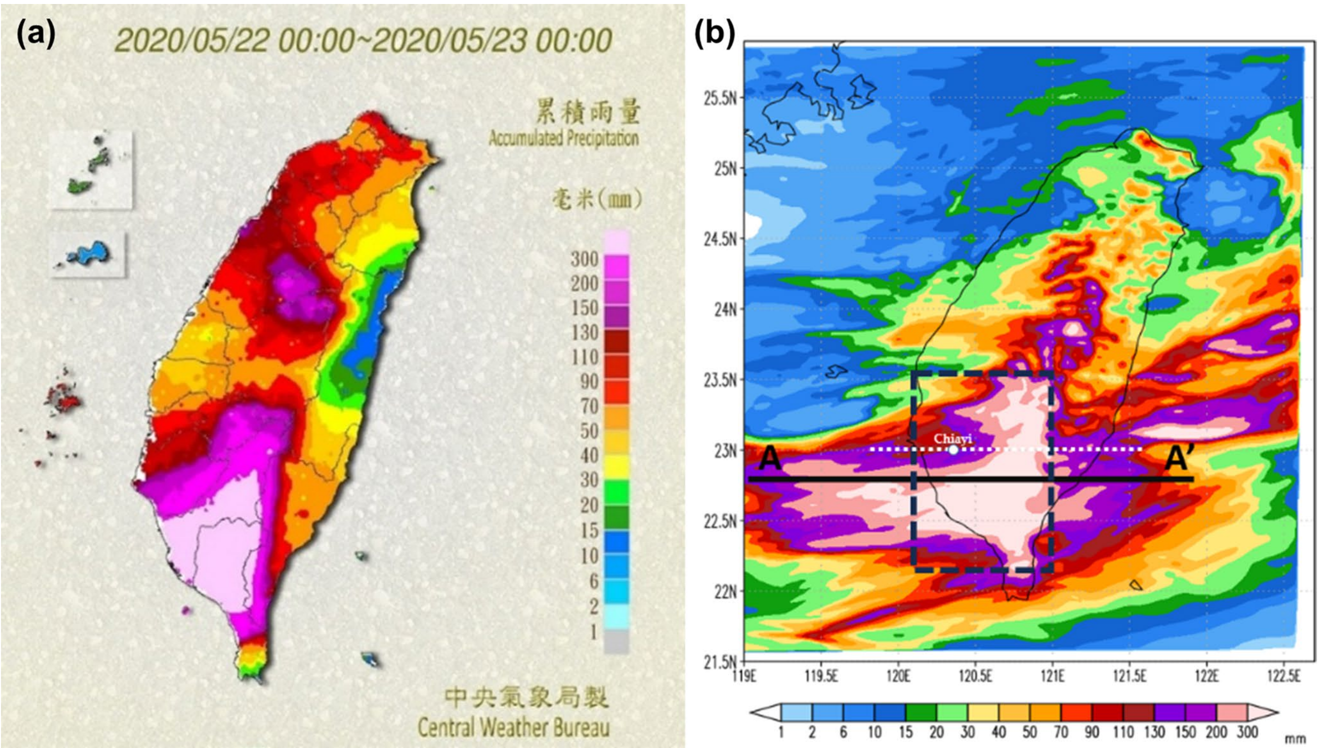

Fig. 13 Comparison of daily accumulated rainfall on May 22, 2020, between observations and numerical simulations. **a** observed results from the CWA, and **b** WRF numerical simulation results. The color shading corresponds to accumulated rainfall (mm) as indicated by the color bar on the right(a) and below(b). The black solid line AA' (22.75°N) represents the location passing through Qiaotou District, Kaohsiung City. The black dashed box marks the area from 120.2°E to 121°E and 22.25°N to 23.5°N. The white dotted line is the latitude line passing through Chiayi City

windward side. This indicates that mountains above 2000 m can disrupt the development of the MCS and effectively block moisture transport.

Overall, under the influence of moisture advection brought by low-level southwesterly airflow and upper-level divergence associated with the diffluent flow field, the MCS can rapidly develop due to the effects of the frontal boundary, low-level convergence, and orographic lifting. However, terrain above 2000 m acts as a barrier that intercepts moisture, leading to heavy precipitation on the windward side while inhibiting MCS development and obviously reducing rainfall on the leeward side. This means that changes in the environmental field are closely related to the rapid development of MCS. The intensity of the MCS system is one of the key factors determining the location of heavy rainfall. While terrain effects are not the sole condition for heavy rainfall, their presence provides MCSs with additional opportunities for enhancement under the same environmental conditions, thereby leading to heavy rainfall. However, whether MCSs occur over the ocean or near topography on land, the amount of rainfall they produce is influenced by the quantity and direction of moisture transported by the southwesterly flow, resulting in variability.

In order to more objectively illustrate the relationship between the intensity change, precipitation distribution and terrain effect during the movement of MCS. We use the vertical atmospheric cross-section (Fig. 15a, b) during the average period from 1300 LST to 1900 LST, covering the same area as Fig. 14, to provide an overall explanation of the process from the development to the gradual dissipation of the MCS. In Fig. 15a, it can be observed that as moisture is transported from the ocean to the land by the wind field, it is affected by land friction and topography, causing a reduction in wind speed in the lower levels, which leads to wind field convergence and subsequent moisture uplift. As the moisture continues to be transported further inland,

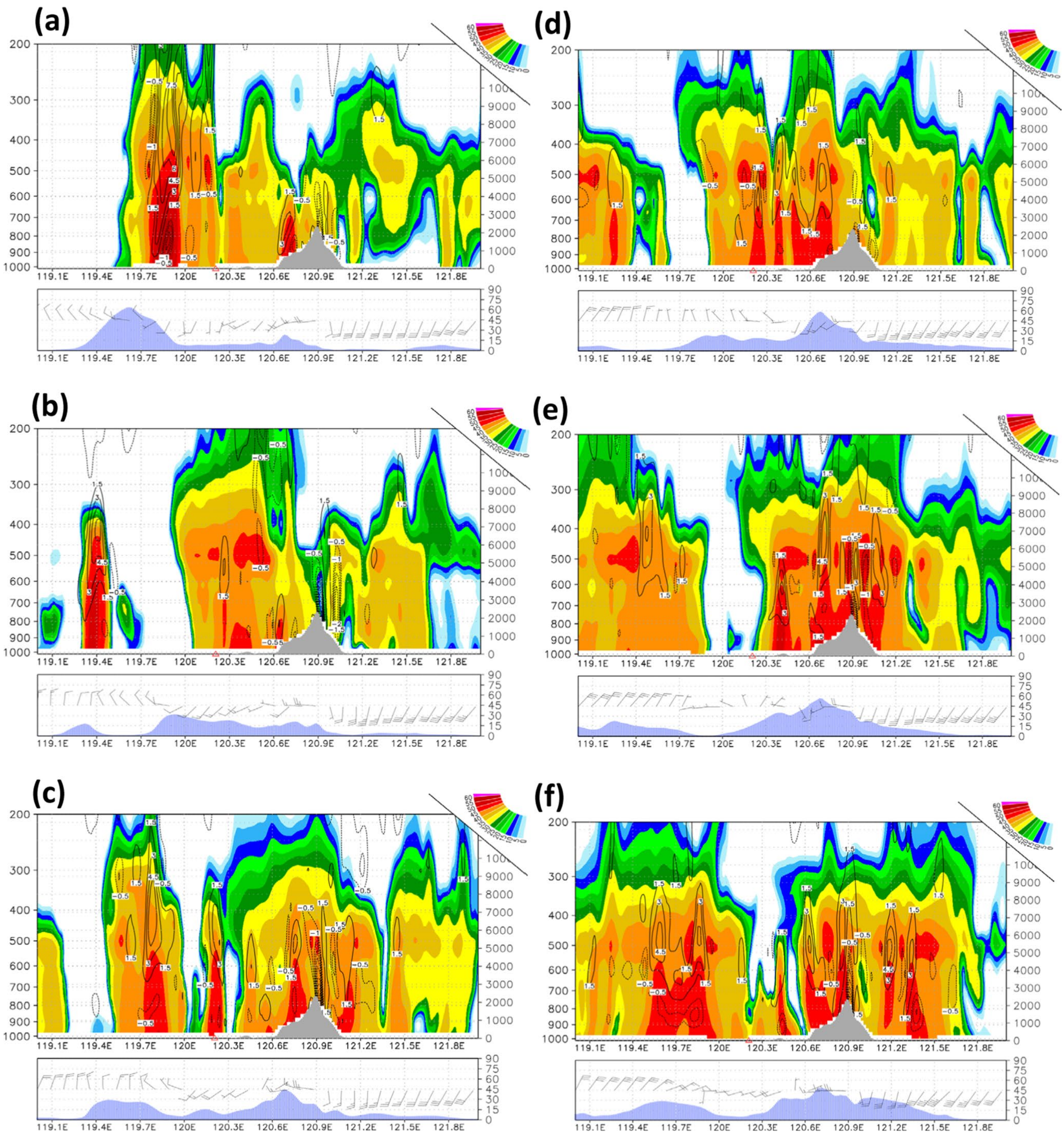

Fig. 14 Time series of AA' radar reflectivity, precipitation amount, horizontal and vertical velocity from 13 to 18 LST (corresponding to a to f) on May 22 in Figure 13b. The colored shading represents radar reflectivity intensity (dBZ) corresponding to the color scale in the upper right corner. The blue area at the bottom indicates the average precipitation amount, with the total precipitation corresponding to the scale on the right. Wind barbs represent the environmental wind field at a height of 10 meters. The contour lines within the colored shading indicate vertical velocity (m s^{-1}), with contour intervals of 1.5 m s^{-1}. The gray areas in the image represent the terrain, and the red hollow triangles indicate the location of the western coastline

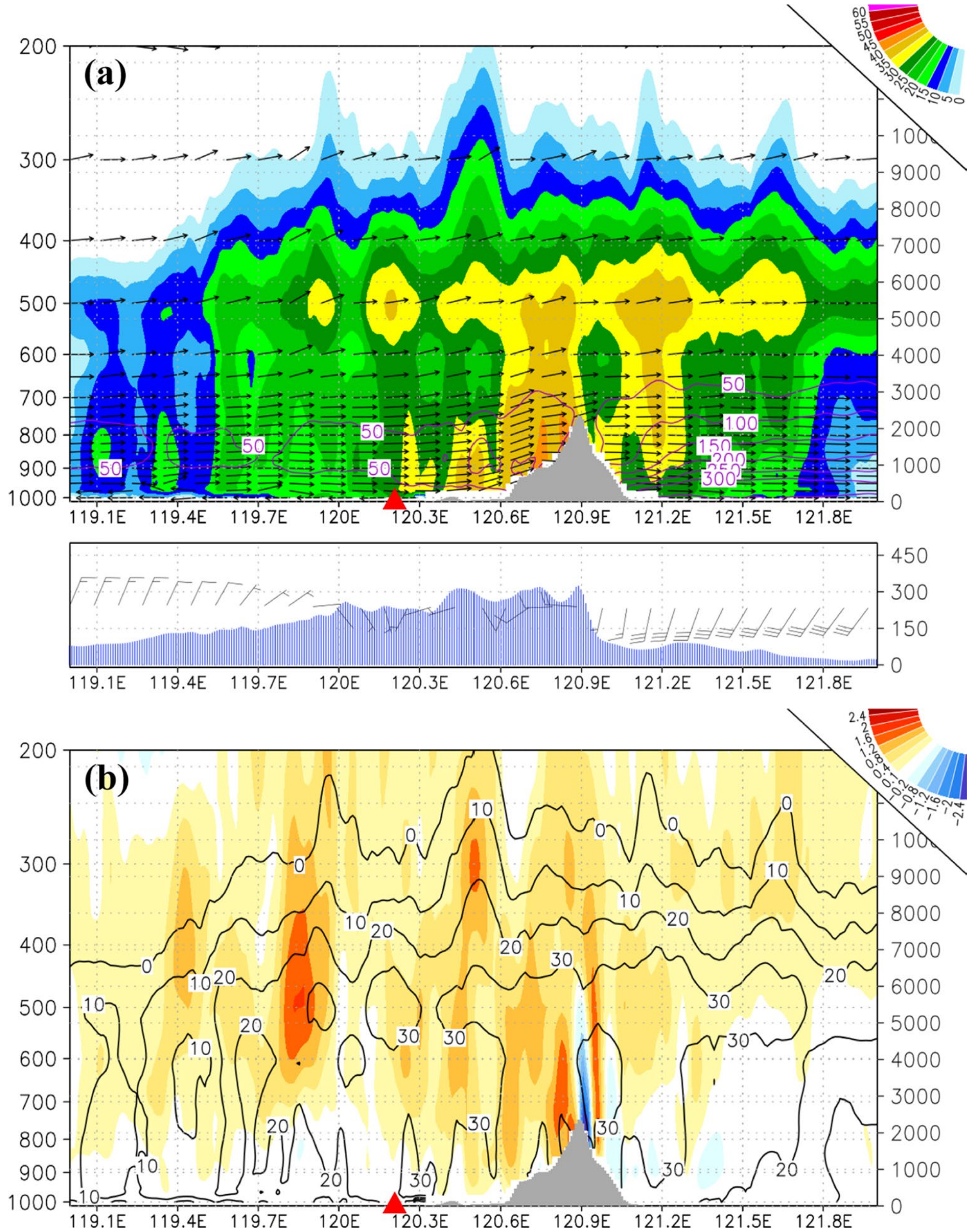

Fig. 15 Same as Fig. 14 but for the vertically averaged cross-section from 0500 LST to 1900 LST on May 22. **a** Arrows indicate the composite wind vectors (u and w). **b** Shaded colors represent vertical motion speed (m s−1) corresponding to the fan-shaped color bar at the upper-right corner, while contour lines represent radar reflectivity (dBZ) from panel (a) at 10 dBZ intervals. The gray areas in the image represent the terrain, and the red triangles indicate the location of the western coastline

it encounters sloped terrain, which induces further uplift. As a result, stronger radar reflectivity values are observed over the terrain (Fig. 15a). Therefore, the most vigorous convective development tends to occur in the upstream regions of the terrain.

This finding is consistent with Houze (2012), who found that as mountain height increases, the resistance to low-level airflow intensifies, making it more difficult for the flow to cross the mountain peak. Consequently, stronger vertical lifting occurs in the upstream region, effectively expanding the "actual scope of influence" of the mountain on the airflow. This study further reveals that, in this case, the influence of terrain on the upstream vertical motion of the airflow extended approximately 150 km upstream from the highest point of the terrain (2000 m). Consequently, stronger radar reflectivity values and accumulated rainfall were observed along the terrain slopes.

Additionally, as shown in Fig. 15a, on the left windward side of the terrain, the environmental wind field is dominated by north-northeast to northeasterly winds. When approaching the terrain, easterly winds will appear due to the influence of local circulation. In contrast, the leeward side (right side) showed south-southwesterly winds. This seems to show that because the terrain height exceeds 2000 m, the airflow cannot cross the mountains, thus blocking the northeasterly wind. However, judging from the average wind field, it is mostly westerly. Corresponding to the averaged vertical motion (Fig. 15b), it can be observed that the windward side (left side of the terrain) predominates upward motion. The areas with stronger radar reflectivity in Fig. 14a, where latent heat release is more obvious, coincide with the regions of the strongest upward velocity.

On the leeward side (right side of the terrain), aside from strong vertical oscillations resembling gravity waves near the mountain peak, weak subsidence dominates below 2000 m. This indicates that while the convective system and southwesterly airflow lack sufficient kinetic energy to cross the terrain, the westerly environmental airflow above 1500 m still flows over the terrain. This flow triggers vertical motions resembling gravity waves, leading to subsidence on the leeward slope. From the above discussion, we can understand that the intensity of a MCS is influenced not only by dynamic mechanisms in the environmental field but also by surface friction, which alters wind speed and subsequently affects the strength of the MCS. Additionally, terrain effects must occur within a specific range to induce the uplift of moisture, which in turn leads to heavy precipitation. In other words, a relatively weak MCS may be enhanced by terrain; however, the extent of this enhancement and its physical relationship with terrain and heavy rainfall remain somewhat uncertain. This is because the moisture supply in the environmental airflow may become one of the key factors under such circumstances.

To understand the impact of complex terrain (varying terrain elevations) on precipitation during the movement of sever rainfall echoes associated with MCSs into Taiwan from the west-northwest to the east-southeast, this study selected vertical cross-sections on the southern Central Mountain Range. The cross-sections region from 23°N (Liugui District, Kaohsiung City) to 22.125°N (Shimen Elementary School, Mudan Township, Pingtung County) at intervals of 0.125° (approximately 13.8 km) (Figs. 4 and 16). Using the 24-hour average rainfall on May 22, the study investigates airflow differences and rainfall distribution before and after the MCS crossed the terrain. Based on the analysis of average moisture variations before and after crossing the terrain in Fig. 16, the vertical cross-section at 11’ (Fig. 16a) shows that the intensity of MCS development over the Taiwan Strait fluctuated, resulting in varying precipitation amounts over the ocean. While precipitation amounts were occasionally slightly above the average on the farthest left side, most of the time, they remained below average. However, upon entering the land, precipitation amounts near the terrain consistently exceeded the average. As moisture passed over the high terrain with an elevation of approximately 2500 m, the maximum accumulated rainfall occurred around 2000 m on the windward slope. The rainfall in this region was more than twice the average amount observed before encountering the terrain. The average maximum rainfall was located at the first mountain peak on the left side of the terrain. Due to the high precipitation on the windward side, the overall average was elevated, but rainfall on the leeward side was consistently below the average. In the vertical cross-section at 22’ (Fig. 16b), the average rainfall over the Taiwan Strait was similar to that in Fig. 16a. However, after the MCS moved onto the western land of Taiwan, rainfall amounts exceeded the average, with two distinct peaks observed. This phenomenon is likely attributed to the steeper terrain in this region, which enhanced the orographic lifting effect. The average maximum rainfall at this location still occurred at the first mountain peak on the left side of the terrain. Similar to Fig. 16a, rainfall on the leeward side was below average. In the vertical cross-section at 33’ (Fig. 16c), the average rainfall over the Taiwan Strait was similar to that in Fig. 16a and b, two weak disturbances with below-average rainfall were observed.

As moisture moved inland and passed over terrain that transitioned from gentle slopes to steeper slopes, two peaks in rainfall intensity were observed over the land, with the maximum occurring at the mountain peak in the gentler terrain. At this time, the deviation below the average rainfall on the leeward side increased. At lower latitudes (44’, Fig. 16d), the average rainfall over the Taiwan Strait was close to the mean, with minimal fluctuations. After the moisture entered the land, below-average rainfall began to appear. As the terrain became steeper again, the increase in average rainfall closely followed the terrain’s shape but was slightly ahead of the terrain’s position. At this time, the maximum rainfall similarly occurred at the first mountain peak on the left side. Meanwhile, the deviation below the average rainfall on the leeward side became even larger. This situation is consistent with the findings of Tai et al. (2020), which showed that the southwesterly flow carries a large amount of moisture and, when it encounters the Central Mountain Range of Taiwan, is forced to ascend. This leads to the rapid uplift of moist air, which further intensifies convective systems and subsequently increases precipitation intensity. Furthermore, the results also align with the observation that the leeward side receives less precipitation compared to the windward side.

When the terrain elevation ranged between 1000 m and 2000 m (Fig. 16e and f), the average rainfall closely matched the terrain’s contours. Initially, the rainfall slightly led the terrain’s position (55’, Fig. 16e) but gradually followed it (66’, Fig. 16f), and the maximum rainfall consistently occurred at the mountain peaks. At this time, the average rainfall over the Taiwan Strait remained below the average in most areas, but the fluctuations increased. On the leeward side, rainfall was consistently below the average, though the deviation from the mean gradually decreased. When the terrain elevation dropped below 600 m (Fig. 16g and h), the average maximum rainfall consistently occurred at the mountain peaks and was generally aligned with the

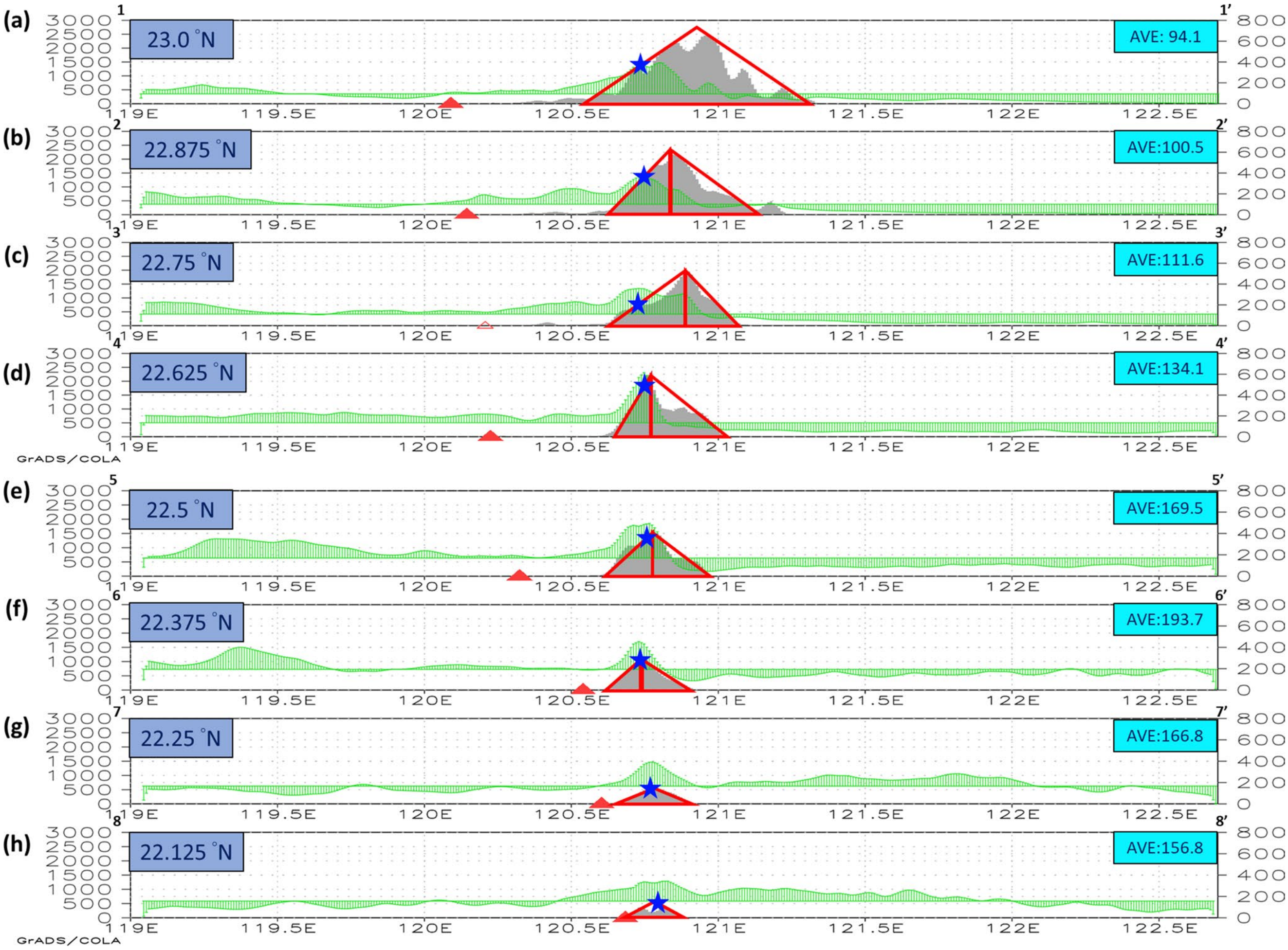

Fig. 16 Diagram of the 8 different terrain vertical cross-sections from west to east and the average accumulated rainfall distribution on May 22 in Figure 4. Green shading represents the accumulated rainfall for May 22, with the horizontal green line indicating the average value for each panel, corresponding to the scale on the right (the value shown in the blue box at the upper-right corner). Areas above the green horizontal line represent rainfall above the average, while areas below indicate below the average. Red triangles mark the boundary between the Taiwan Strait and the western landmass of Taiwan. Gray shading illustrates the vertical profile of the terrain (corresponding to the left scale, in meters), with the red line following the terrain shape. Dark blue stars indicate the elevation where the maximum accumulated rainfall occurred

terrain. On the leeward side, however, rainfall began beyond the average. The leeward subsidence effect only decreases precipitation when the terrain is relatively high for the average rainfall. Additionally, the rainfall amount varies with terrain elevation.

Overall, abundant moisture carried by the southwesterly airflow, under the atmospheric structure of the Mei-yu front, led to the formation and development of MCSs. After the MCSs moved onto the southwestern land of Taiwan, the complex terrain obviously influenced rainfall distribution. In the region we selected, from north to south, as the terrain elevation decreased, average rainfall increased gradually, but it began to decline once the terrain dropped below 1100 m (Fig. 16f). The rise and fall of average rainfall are associated with the amount of precipitation produced by the MCS before encountering the terrain, the intensity of its development, and the obvious impact of the terrain on the intensity and precipitation of MCSs on the windward side.

The most areas of the Taiwan Strait were below the average, with only localized regions influenced by mature deep convection within the MCS, where heavy precipitation caused the average local rainfall to exceed the overall average. When the MCS moved onto land and encountered terrain over 2000 m in elevation (Fig. 16a-d), the average rainfall was consistently above the overall average due to the influence of the terrain. However, as the terrain was excessively steep (Fig. 16d), below-average rainfall could occur near the coastline, some distance downstream from the terrain. On the leeward side, where the terrain exceeds 1000 m in elevation (Fig. 16a–f), the average rainfall was below the overall average due to the blocking effect of the terrain. As the terrain height decreased, the deviation below the average rainfall on the leeward side gradually declined. When the terrain was below 600 m (Fig. 16g and h), maximum rainfall over land was observed at the mountain peaks, while rainfall on the leeward side exceeded the average. Across all terrain elevations (Fig. 16a–h), maximum rainfall locations, influenced by complex terrain, appeared either at the local highest points of the terrain or on relatively gentle slopes and mid-mountain areas affected by steep terrain.

4 Summary and Discussion

At 0800 LST on May 22, 2020, the MCSs exhibited the most vigorous cloud development from the northern Taiwan Strait to areas near Hong Kong and Hainan Island. A high moisture flux extended from the South China Sea, across Taiwan, the Ryukyu Islands, and the southern waters of Japan, reaching the west coast of the United States, forming a moisture transport band resembling an "atmospheric river." This abundant and moist southwesterly airflow provided sufficient moisture to support convective development around Taiwan. On that day, the eastward movement of the trough at 500 hPa enhanced positive vorticity, which, combined with upper-level divergence at 200 hPa, strengthened the dynamic development mechanism of the MCS. Radar reflectivity on that day revealed two northeast-to-southwest-oriented linear convective systems: one occurring from 0100 LST to 0300 LST and the other from 1400 LST to 1600 LST. These systems moved from the Taiwan Strait toward land, where they were influenced by the complex terrain of southwestern Taiwan, resulting in extreme rainfall.

On that day, the LLJ rich in moisture was observed at Pratas Island, Penghu, and Pingtung Airport, as indicated by their soundings. The analysis revealed an atmospheric environment classified as "extremely unstable with potential for thunderstorms," attributed to the MBLJ originating from the South China Sea. Additionally, the LCL at Pingtung Airport was only about 67 m, the CCL was approximately 714 m, and the LFC was as low as 70 m. These low levels suggest that air parcels required minimal external forcing to reach free convection, creating favorable conditions for convective system development and facilitating the intensification of the MCS. The analysis of the Mei-yu front during the early morning strengthened and revealed obvious mid-to-upper-level convective layer wind speeds and vertical wind shear in the mid-to-lower levels. Coupled with the presence of a LLJ, these conditions caused an unstable atmospheric environment with high CAPE, favoring the development of deep convection within the system. In the post-frontal environment, the lower-level air was relatively dry and cool, resulting in lower instability and CAPE, which limited the depth of convection within the system. From the observational data, when the moist and strong southwesterly airflow was lifted along the leading edge of the Mei-yu front, MCSs formed and rapidly developed over the ocean. The development during the afternoon was faster than during the early morning. As the MCS moved east-southeastward over land, the complex terrain of southwestern Taiwan further enhanced convective precipitation, ultimately leading to heavy rainfall in the region.

Additionally, to verify the accuracy of the model simulation of the offshore wind field and confirm that the simulated southwesterly flow can reproduce the characteristics of the LLJ over the southwestern offshore region of Taiwan as observed, we compared satellite-observed wind speeds from ASCAT with the simulation results in the same region. The results showed good simulation performance, indicating that the model can accurately capture the LLJ associated with the southwesterly flow. To understand which environmental factors obviously influence the development of MCS over the southwestern sea area of Taiwan, we calculated correlation coefficients and averaged grid data from 0500 to 1300 UTC over key regions affecting the intensity of the southwesterly flow. The results revealed that the intensity of MCS radar echoes is primarily determined by dynamic factors such as low-level wind field convergence and high-level divergence, vertical motion, and thermodynamic conditions including moisture supply and phase transitions. Among these, low-level wind field convergence, moisture supply, and the latent heat released from intense precipitation due to condensation have the most obvious impact on MCS radar echo intensity. This suggests that for MCS formation over the southwestern offshore region of Taiwan during the 0500 to 1300 UTC period, the moisture transport provided by the LLJ within the southwesterly flow, along with low-level wind field convergence and uplift-induced condensation, are the key factors influencing MCS intensity variations. This is also a key factor contributing to the uncertainty in the physical connection between MCS intensity variations, terrain effects, and heavy precipitation.

The simulated and observed distribution characteristics of the heavy rainfall over Taiwan on May 22 were generally consistent, with Chiayi (23.5°N) marking the approximate boundary. North of Chiayi, particularly in northwestern Taiwan, the simulated total rainfall was lower than the observed values. Overall, the daily accumulated rainfall distribution from the simulation shows that in areas north of Chiayi, rainfall increased continuously from the coastline inland, with the highest accumulation observed in the mountainous regions. The area south of Chiayi has a much larger area of heavy rainfall than the area north of Chiayi. This indicates that as the Mei-yu front oscillated over Taiwan, the MCS caused two distinct rainfall patterns in the north and south of Chiayi. Although Chiayi served as the dividing line for these two rainfall types, the maximum rainfall still occurred in the mountainous regions, highlighting the amplifying effect of Taiwan's complex terrain on regional precipitation.

To investigate the vertical variation of rainfall within the MCS as it moved from the ocean to land, we selected Qiaotou District in Kaohsiung City (22.75°N) for an averaged vertical cross-section analysis. The results indicate that as moisture was transported from the ocean to land by the wind field, it was affected by surface friction and topography, leading to a reduction in wind speed at lower levels and a subsequent decrease in horizontal moisture flux precipitation amount. However, as the moisture continued moving inland, it encountered terrain slopes, causing uplift. This uplift resulted in stronger radar reflectivity observed above the terrain, though the most vigorous convective development occurred upstream of the terrain. This is consistent with the findings of Houze (2012), which showed that as mountain height increases, the resistance to low-level airflow becomes greater, making it harder for the airflow to pass over the mountain peak. This leads to stronger vertical lifting effects in the upstream region, effectively extending the "actual influence range" of the terrain on the airflow. This study further reveals that the influence of terrain on the vertical motion of airflow in the upstream region extended more than 150 km from the highest point of the terrain (2000 m). When the terrain exceeded 2000 m in elevation, the airflow could not cross the mountain, and on the leeward side, was primarily dominated by the environmental wind field. Aside from vertical oscillations and descending motions resembling gravity waves near the mountain peak on the leeward side, most areas below 2000 m exhibited weak descending motion.

To further understand the impact of the complex terrain on the southern Central Mountain Range (at varying elevations) on intense rainfall echoes associated with MCSs as they moved over Taiwan, this study selected eight vertical cross-sections. Based on the 24-hour average rainfall on May 22, the study analyzes airflow differences and rainfall distribution before and after the MCS crossed the terrain. The results show that abundant moisture carried by the southwesterly airflow, under the atmospheric structure of the Mei-yu front, led to the formation and development of MCSs. After moving onto the southwestern landmass of Taiwan, the MCSs were influenced by the complex terrain. In the analyzed region, the average rainfall increased progressively from north to south as terrain elevation decreased. However, once the terrain dropped below 1100 m, the average rainfall started to decrease. The average rainfall over most of the Taiwan Strait was below the overall average, except in localized regions influenced by sever rainfall induced by deep convection within the MCS, where the average rainfall exceeded the average. However, after the MCS moved onto land and encountered terrain higher than 2000 m in elevation, the influence of the terrain caused the average rainfall to consistently exceed the average, with maximum rainfall observed near the windward slopes of the mountainous regions on Taiwan's western land. When the terrain was excessively steep, below-average rainfall could occur near the coastline, some distance downstream from the terrain. As the terrain exceeded 1000 m in elevation, the leeward side experienced below-average rainfall due to the blocking effect of the terrain. With the terrain elevation decreased, the deviation of rainfall below the average on the leeward side gradually diminished. The location of maximum average rainfall, influenced by complex terrain, tends to appear at the highest local positions of the terrain or relatively gentle slopes and mid-mountain areas affected by steep terrain. When the terrain is below 600 m, the maximum rainfall over land occurs at the mountain peaks, while rainfall on the leeward side exceeds the average.

Acknowledgements During the preparation of this work the author(s) use [Google Translate/ChatGpt/Grammarly] to translate, proofread, and check grammar. After using this tool/service, the author(s) reviewed and edited the content as needed and take(s) full responsibility for the content of the publication. Thanks to National Taiwan University for providing weather instruments and AI-related resources.

Author Contributions Conceptualization, JPH; Formal analysis, CYC, and JPH; Funding acquisition, JPH; Investigation, CYC, and JPH; Methodology, CYC, and JPH; Project administration, JPH; Software, CYC and JPH; Supervision, JPH; Statistic analysis, CYC; Validation, JPH; Visualization, CYC, and JPH; Writing—original draft, JPH, CYC, and PDJ; Writing—review and editing, JPH, CYC, and PDJ.

Funding This research was supported by National Science and Technology Council (NSTC) of Taiwan under grants, NSTC 112-2123-M-002-006, NSTC 113-2123-M-002-018 and NSTC 113-2124-M-002-015.

Data Availability The WRF model and its user's guide are open to researchers and available at https://www.mmm.ucar.edu/models/w, and the NCEP GFS data are available at http://rda.ucar.edu/datasets/ds335.0/#!description.

Declarations

Conflict of Interest The authors declare that there are no conflicts of interest associated with this study.

References

Beljaars, A.C.M.: The parametrization of surface fluxes in large-scale models under free convection. Q. J. R Meteorol. Soc. **121**, 255–270 (1995)

Chen, G.T.-J.: Mesoscale features observed in the Taiwan Mei-Yu season. J. Meteorol. Soc. Jpn. **70**, 497–516 (1992)

Chen, G.T.-J.: Research on the phenomena of Meiyu during the past quarter century: An overview. In: Chang, C.-P. (ed.) East Asian Monsoon, pp. 357–403. World Scientific, Singapore (2004)

Chen, C.-S., Chen, Y.-L.: The rainfall characteristics of Taiwan. Mon Weather Rev. **131**, 1323–1341 (2003). https://doi.org/10.1175/1520-0493(2003)131<1323:TRCOT>2.0.CO;2

Chen, Y.-L., Hui, N.B.-F.: Analysis of a shallow front during the Taiwan area mesoscale experiment. Mon Weather Rev. **118**, 2649–2667 (1990)

Chen, Y.-L., Hui, N.B.-F.: Analysis of a relative dry front during the Taiwan area mesoscale experiment. Mon Weather Rev. **120**, 2442–2468 (1992)

Chen, C., Tao, W.-K., Lai, G.R.S., Lan, S.: The interaction of the upper- and low-level jets in the development of mesoscale convective systems in a Mei-Yu front: MM5 model simulations. Proceedings of the Conference on Weather Analysis and Forecasting and Marine Meteorology, Taipei, Taiwan, pp. 294–299. https://photino.cwa.gov.tw/rdcweb/lib/cd/cd01conf/dissertation/1996/39%20The%20interaction%20of%20the%20upper-and%20low-level%20jets%20in%20the%20development%20of%20mesoscale%20convective%20systems%20in%20a%20Mei-Yu%20front.pdf (1996)

Chen, C.-S., Chen, Y.-L., Liu, C.-L., Lin, P.-L., Chen, W.-C.: Statistics of heavy rainfall occurrences in Taiwan. Wea Forecast. **22**, 981–1002 (2007). https://doi.org/10.1175/WAF1033.1

Chen, Y.-L., Tu, C.-C., Hsiao, F., Chen, C.-S., Lin, P.-L., Lin, P.-H.: An overview of low-level jets (LLJs) and their roles in heavy rainfall over the Taiwan area during the early summer rainy season. Meteorology. **1**, 64–112 (2022). https://doi.org/10.3390/meteorology1010006

Chien, F.-C.: The role of Southwesterly flow in MCS formation during a heavy rain event in Taiwan on 12–13 June 2005. TAO: Terr. Atmos. Ocean. Sci. **26**, 411–429 (2015). https://doi.org/10.3319/TAO.2015.03.11.01(A)

Chien, F.-C., Chiu, Y.-C.: Factors leading to heavy rainfall in Southern Taiwan in the early Mei-Yu season of 2020. Mon Weather Rev. **151**, 1885–1908 (2023). https://doi.org/10.1175/MWR-D-22-0226.1

Chou, M.-D., Suarez, M.J.: A solar radiation parameterization for atmospheric studies. NASA Tech. Memo. **NASA/TM–1999–104606/VOL15**, 40–pp (1999)

Colle, B.A.: Sensitivity of orographic precipitation to changing ambient conditions and terrain geometries: An idealized modeling perspective. J. Atmos. Sci. **61**, 588–606 (2004)

Cornejo, I.C., Rowe, A.K., Rasmussen, K.L., DeHart, J.C.: Orographic controls on extreme precipitation associated with a Mei-Yu front. Mon Wea Rev. **152**, 531–551 (2024). https://doi.org/10.1175/MWR-D-23-0170.1

Ding, Y.-H.: Summer monsoon rainfalls in China. J. Meteorol. Soc. Jpn. **70**, 337–396 (1992)

Henny, L., Thorncroft, C.D., Hsu, H., Bosart, L.F.: Extreme rainfall in taiwan: Seasonal statistics and trends. J. Clim. **34**, 4711–4731 (2021). https://doi.org/10.1175/JCLI-D-20-0999.1

Hersbach, H., Stoffelen, A.: Validation of the scatterometer winds using the global ECMWF model. J. Atmos. Ocean. Technol. **17**, 581–590 (2000)

Hong, S.-Y., Dudhia, J., Chen, S.-H.: A revised approach to ice microphysical processes for the bulk parameterization of clouds and precipitation. Mon Weather Rev. **132**, 103–120 (2004)

Hong, S.-Y., Noh, Y., Dudhia, J.: A new vertical diffusion package with an explicit treatment of entrainment processes. Mon Weather Rev. **134**, 2318–2341 (2006)

Houze, R.A. Jr.: Orographic effects on precipitating clouds. Rev. Geophys. **50**, RG1001 (2012). https://doi.org/10.1029/2011RG000365

Jiang, Q.: Precipitation over concave terrain. J. Atmos. Sci. **63**, 2269–2288 (2006). https://doi.org/10.1175/JAS3761.1

Kain, J.S.: The Kain-Fritsch convective parameterization: An update. J. Appl. Meteor. **43**, 170–181 (2004)

Lin, Y.-L.: Mesoscale Dynamics, p. 475. Cambridge University Press (2007). https://doi.org/10.1017/CBO9780511619649

Lin, Y.-L., Chou, C.-H., Chang, Y.-T.: Effects of orography and low-level jets on rainfall distribution during the Mei-Yu season in Taiwan. Mon Weather Rev. **118**, 2002–2021 (1990)

Mlawer, E.J., Taubman, S.J., Brown, P.D., Iacono, M.J., Clough, S.A.: Radiative transfer for inhomogeneous atmospheres: RRTM, a validated correlated-k model for the longwave. J. Geophys. Res. **102**, 16663–16682 (1997)

National Centers for Environmental Prediction (NCEP): NCEP FNL Operational Model Global Tropospheric Analyses, Continuing from July 1999. Research Data Archive at the National Center for Atmospheric Research, Computational and Information Systems Laboratory. Available online: (2015). https://rda.ucar.edu/datasets/ds083.3/ (accessed on March 7, 2025)

Sever, G., Lin, Y.: Dynamical and physical processes associated with orographic precipitation in a conditionally unstable uniform flow: Variation in basic wind speed. J. Atmos. Sci. **74**, 449–466 (2017). https://doi.org/10.1175/JAS-D-16-0077.1

Tai, S., Liou, Y., Chang, S., Sun, J.: The heavy rainfall mechanism revealed by a terrain-resolving 4DVar data assimilation system—A case study. Mon Wea Rev. **148**, 2307–2330 (2020). https://doi.org/10.1175/MWR-D-19-0244.1

Tu, C.-C., Y.-L. Chen, P.-L. Lin, Du, Y.: Characteristics of the marine boundary layer jet over the South China sea during the early summer rainy season of Taiwan. Mon Weather Rev. **147**, 457–474 (2019)

Tu, C.-C., Chen, Y.-L., Lin, C.-S., Lin, P.-H.: The relationship between the boundary layer moisture transport from the South China sea and heavy rainfall over Taiwan. Terr. Atmos. Ocean. Sci. **31**, 159–176 (2020)

Tu, C., Chen, Y., Lin, P., Huang, M.: Analysis and simulations of a heavy rainfall event associated with the passage of a shallow front over Northern Taiwan on 2 June 2017. Mon Wea Rev. **150**, 505–528 (2022). https://doi.org/10.1175/MWR-D-21-0113.1

Verhoef, A., Stoffelen, A., Portabella, M.: Improving ASCAT wind retrievals using machine learning techniques. Remote Sens. **14**, 3754 (2022)

Wang, S.-Y., Cheng, K.-H., Lee, D.-H., Yang, P.-L.: On the formation and structure of mesoscale convective systems in Taiwan during the Mei-Yu season. J. Atmos. Sci. **47**, 2297–2312 (1990)

Wang, C.-C., Chuang, P.-Y., Chen, S.-T., Lee, D.-I., Tsuboki, K.: Idealized simulations of Mei-Yu rainfall in Taiwan under uniform Southwesterly flow using a cloud-resolving model. Nat. Hazards Earth Syst. Sci. **22**, 1795–1817 (2022)

Watson, C.D., Lane, T.P.: Sensitivities of orographic precipitation to terrain geometry and upstream conditions in idealized simulations. J. Atmos. Sci. **69**, 1208–1231 (2012). https://doi.org/10.1175/JAS-D-11-0198.1

Yu, C., Liu, W., Cheng, L., Lin, C.: Mechanisms of Valley precipitation enhancement over Da-Tun mountain. Mon Wea Rev. **150**, 1851–1871 (2022). https://doi.org/10.1175/MWR-D-21-0195.1